African horse sickness virus NS4 is a nucleocytoplasmic protein that localises to PML nuclear bodies

1.1 Author names

1. Shareen Boughan (ORCiD: 0000-0003-3667-4122)
2. Abraham Christiaan Potgieter
3. Vida van Staden*

1.2 Affiliation

1. Department of Biochemistry, Genetics and Microbiology, University of Pretoria, Pretoria, South Africa.
2. Deltamune (Pty) Ltd, Moraine house-The Braes, 193 Bryanston drive, Bryanston, Gauteng, 2191, South Africa.

   Department of Biochemistry, Focus Area for Human Metabolomics, North-West University, Potchefstroom, South Africa.
3. Department of Biochemistry, Genetics and Microbiology, University of Pretoria, Pretoria, South Africa.

1.3 Corresponding author

**vida.vanstaden@up.ac.za*

1.4 Keyword

African horse sickness virus, AHSV, NS4, PML nuclear bodies, NS1, NS2

1.5 Repositories:

The following sequences are available on Genbank:

MN625126

MN625127

MN625128

MN625129

MN625130

MN625131

MN625132

MN625133

MN625134

2. Abstract

African horse sickness virus (AHSV) is the causative agent of the often fatal disease African horse sickness in equids. The non-structural protein NS4 is the only AHSV protein that localises to the nucleus. Here we report that all AHSV reference and representative field strains express one of the two forms of NS4, i.e. NS4-I or NS4-II. Both forms of NS4 are nucleocytoplasmic proteins, however NS4-I has a stronger nuclear presence whilst NS4-II has a proportionally higher cytoplasmic distribution. A subtype of NS4-II containing a nuclear localisation signal (NLS), named NLS-NS4-II, displays distinct punctate foci in the nucleus. We showed that NS4 likely enters the nucleus via passive diffusion as a result of its small size. Colocalisation analysis with nuclear compartments revealed that NS4 colocalises with promyelocytic leukemia nuclear bodies (PML-NBs), suggesting a role in the antiviral response or interferon signalling. Interestingly, we showed that two other AHSV proteins also interact with nuclear components. A small fraction of the NS1 tubules were present in the nucleus and associated with PML-NBs, this was more pronounced for a virus strain lacking NS4. A component of nuclear speckles, serine and arginine rich splicing factor 2 (SRSF2), was recruited to VIBs in the cytoplasm of AHSV-infected cells and colocalised with NS2. Nuclear speckles are important sites for cellular mRNA transcript processing and maturation. Collectively, these results provide data on three AHSV non-structural proteins interacting with host cell nuclear components that could contribute to overcoming antiviral responses and creating conditions that will favour viral replication.

3. Introduction

African horse sickness (AHS) is a serious arthropod-borne infectious disease affecting Equidae [1]. AHS is endemic to sub-Saharan Africa, with sporadic outbreaks in North Africa and in Europe. AHS has official recognition status from the World Organisation for Animal Health (OIE), and is of major economic importance in southern Africa both due to its high mortality rate and its role in horse trade and movement restrictions. AHS is caused by African horse sickness virus (AHSV) [2], and nine serotypes (AHSV-1 to AHSV-9) have been distinguished [3, 4]. AHSV belongs to the *Orbivirus* genus and the *Reoviridae* family, with bluetongue virus (BTV) defined as the prototype virus of the genus [5]. AHSV is transmitted via *Culicoides* biting midges, specifically *C. bolitinos* and *C. imicola* in southern

Africa [6]. Currently, a polyvalent live attenuated vaccine (LAV) that confers broad protection against all AHSV serotypes is used widely in southern Africa [7, 8]. This same LAV may, paradoxically, place susceptible horses at risk for AHS by reversion to virulence [9]. This vaccine also does not allow for the differentiation of infected from vaccinated animals (DIVA), and has not been licensed for use outside Africa.

Different forms of the disease AHS exist (fever, pulmonary, cardiac and mixed) [1] however symptoms vary between species. No disease is observed in the reservoir host (zebra) and African donkeys seldom show clinical signs, but AHS can cause up to 95% mortality in fully susceptible horses. In horses the outcome of the infection depends on a variety of viral and host factors, and unravelling the specific contributions of AHSV proteins to virulence, and host immune responses to disease susceptibility, remain a major challenge [10].

AHSV is a non-enveloped virion composed of three concentric layers [11] formed by seven structural proteins (VP1 to VP7). The capsid encloses ten double-stranded RNA (dsRNA) genome segments (Seg-1 to Seg-10) encoding the structural proteins plus four non-structural proteins (NS1 to NS4). The outer layer of the virus particle consists of the serotype-specific antigen (VP2) and the protein involved in membrane permeabilisation (VP5). The middle layer consists of VP7 and VP3 forming the core, which contains the transcription complex (VP1, VP4 and VP6) and the dsRNA genome [12]. Non-structural proteins play core roles in the viral replication cycle. NS1 assembles into tubules of unknown function in the cytoplasm [13], which are a hallmark of orbivirus infections. BTV NS1 is involved in upregulating protein synthesis from viral mRNAs during infection [14], although this was recently shown to be unrelated to its tubulisation [15]. NS2 forms dense granular cytoplasmic viral inclusion bodies (VIBs), which act as sites for viral genome replication and new particle assembly [16]. The membrane-associated non-structural proteins NS3/3A mediate intracellular virus trafficking and release but are not essential for virus replication in mammalian cells [17-19].

NS4 is the smallest of the orbivirus non-structural proteins, and its function in AHSV remains undescribed. The AHSV NS4 open reading frame (ORF) is present on Seg-9, overlapping the larger ORF encoding VP6 in the +1 frame [20] . All AHSV serotypes encode NS4 [21] and the AHSV NS4 ORF is the longest of all orbivirus NS4 ORFs [22]. Based on AHSV Seg-9 nucleotide and NS4 amino acid (aa) sequence comparisons two main clades were identified, and the type of NS4 within each of these designated NS4-I and NS4-II respectively. On average NS4-I and NS4-II sequences share 52% amino acid identity, and NS4-II (154 aa) is larger than NS4-I (144 aa). A subset of strains within the NS4-II clade encodes a longer variant of NS4-II with a 15 aa N-terminal extension containing a typical nuclear localisation signal (NLS) sequence [21].

NS4 is successfully expressed in AHSV-, BTV- and Great Island Virus (GIV)-infected mammalian cells, however the expression of NS4 in insect cells has only been confirmed for BTV [21, 23]. Immunohistochemistry on AHSV-infected horse tissue detected NS4 in microvascular endothelial cells (heart and lung) and with a strong nuclear distribution in stellate-shaped dendritic macrophage-like cells (red pulp of the spleen). Orbiviruses replicate exclusively in the cytoplasm, and NS4 is the only viral protein that has been detected in the nucleus. In BTV, it is suggested that NS4 enters the nucleus using a basic domain region on the N-terminal [23]. AHSV NS4 could potentially utilise the NLS for nuclear import [24, 25] when present, alternatively it could passively move through the nuclear pores as a result of its small size [26]. BTV NS4 specifically colocalises with the nucleolus [23], however AHSV NS4 does not [21].

Both AHSV and BTV NS4 were shown to bind to double-stranded DNA (dsDNA), potentially via helical structures, suggesting a role in regulation of host gene expression [21, 22]. It was subsequently confirmed that BTV NS4 modulates the host interferon (IFN) response by downregulating mRNA levels of type I IFN and interferon-stimulated genes, and specifically downregulates the activity of a number of promoters. This inhibitory effect of BTV NS4 was directly related to its nucleolar localisation in a strain-specific fashion [27]. NS4 is dispensable for BTV replication in cell lines that lack competent innate immune systems and in IFN-α/β receptor $^{-/-}$ (IFNAR$^{-/-}$) mice, but confers a replication advantage on BTV in IFN-treated cells and *in vivo* in sheep. BTV NS4 therefore acts as an IFN antagonist and virulence factor [23, 27].

AHSV NS4 is much larger than BTV NS4, less conserved within the serogroup, and shows nuclear and cytoplasmic distribution but does not localise to the nucleolus. For viruses that replicate in the cytoplasm, viral proteins that localise to the nucleus often counteract the host immune response or take over the host machinery by targeting subnuclear compartments such as nuclear speckles, promyelocytic leukemia nuclear bodies (PML-NBs) or Cajal bodies [28]. In this study we carried out an in-depth comparison of NS4 expression and intracellular localisation across all AHSV serotypes, investigated whether the protein's cellular distribution profile is influenced by other viral proteins or the viral replication cycle, and identified whether NS4 interacts with any specific intranuclear compartments. The results shed some light on the potential role of NS4 in the AHSV life cycle.

4. Methods

Cells and viruses

BSR-T7 (BSR cells which constitutively express T7 polymerase) (used with permission from Ulla Bucholz, Department of Clinical Virology, Federal Research Center for Virus Diseases of Animals, Tübingen, Germany) [29] or BSR cells (a kind gift from Piet van Rijn, Wageningen Bioveterinary Research, The Netherlands) were maintained as monolayers in Minimum Essential Medium (MEM) with Earle's salts, L-Glutamine and $NaHCO_3$ (Lonza; BE12-611F) supplemented with 5% fetal bovine serum (FBS, Gibco®), 1% non-essential amino acids (NEAA, Lonza), 1% penicillin and streptomycin (pen/strep) and 1.2% fungizone (Highveld Biologicals). HeLa cells (kindly provided by Michelle Visagie, Department of Physiology, University of Pretoria) were grown as monolayers in Dulbecco's Modified Eagle Medium (DMEM) with 4.5 g/L Glucose and L-Glutamine (Lonza) supplemented with 10% FBS, 1% NEAA, 1% pen/strep and 1.2% fungizone. All mammalian cell lines were incubated at 37°C with 5% CO_2 and 90% humidity.

Spodoptera frugiperda (Sf9) cells (ATCC CRL-1711) were maintained in suspension by shaking at 120 rpm or grown as monolayers in TC-100 medium (Lonza, BE02-011F) supplemented with 10% FBS, 1% pen/strep and 1.2% fungizone and incubated at 28°C.

The nine AHSV OIE reference strains have been described previously [30]. Low passage AHSV reference strains were obtained from the OIE reference centre at the ARC-Onderstepoort Veterinary Institute (OVI) in 2008 with permission from Dr Truuske Gerdes. Recent South African field isolates representing each AHSV serotype were from the Deltamune collection (see Table 1). The serotypes of the field isolates were determined by real-time RT-PCR assays targeting Seg-2 [31]. Virus stocks were obtained by infection of BSR-T7 cells at a low multiplicity of infection (MOI), harvested when full cytopathic effect (CPE) was observed and stored at 4°C. Virus titers were determined by endpoint dilution and expressed as $TCID_{50}$/ml (50% tissue culture infective dose per millilitre).

Rescue of rAHSV-5ΔNS4

The rescue of a 'synthetic' AHSV-5 from the virulent reference strains AHSV-5 isolate HS 30/62 by reverse genetics has been described previously [32]; when used here it is referred to as rAHSV-5. This virus was used in this study as it was shown to be virulent in five control horses at Deltamune during vaccine trials (results not shown) (Patent WO 2016/071850) [33] and therefore represents wild-type virulent AHSV. In addition, we generated a rAHSV-5ΔNS4 deletion mutant that did not express NS4. A cDNA copy of AHSV-5 Seg-9 was synthesised containing the nucleotide substitutions T194C, T197C, T305C, T377C, T401C, T449C, T452C, T455C, T467C, A551G and cloned into plasmid pSMART-T7 (Genscript Corporation). These modifications resulted in changing the NS4 start codon and the eight downstream methionine codons to threonine codons and the ninth methionine to a serine. Additionally, two stop codons were incorporated at amino acids 6 and 47 by substitution of nucleotides

G209A and T332A using a QuikChange site directed mutagenesis kit (Agilent). None of these changes affected the sequence of the VP6 protein expressed from an alternative reading frame on Seg-9. For the plasmid-based reverse genetics rescue, monolayers of BSR-T7 cells were subjected to transfection. BSR-T7 cells were transfected with 5 µg of an equimolar mix of expression plasmids, combined with 5 µg of an equimolar mix of transcription plasmids in pSMART-T7, in Lipofectamine 2000 (LF2000) (Thermo Fisher). The expression vector phCMV dream was a kind gift from Piet van Rijn. Open reading frames encoding VP1 (Genbank KM886344), VP3 (Genbank KM886346), VP4 (Genbank KM886347), VP6 (Genbank KM886352), VP7 (Genbank KM886350) and NS2 (Genbank KM886351) of virulent AHSV-5 were codon were optimised for expression in Syrian golden hamster cells, synthesised and cloned into BsmBI sites of phCMV dream by Genscript Corporation. The transcription plasmids are similar to those described previously [34]. The transfection mix was added dropwise to cells containing optiMEM® and incubated for 24 hours at 37°C. Cells were then passaged once and harvested when 100% CPE was visible. Virus was stored at 4°C.

Sequencing of Seg-9

BSR-T7 cells were infected with AHSV at an MOI of 0.1 and harvested when full CPE was observed. Total RNA was purified using TRIzol Reagent (Invitrogen), and single-stranded RNA was removed using 2 M lithium chloride. Complementary DNA (cDNA) was synthesised from isolated dsRNA using the RevertAid™ First Strand cDNA synthesis kit and random hexamer primers (ThermoFisher Scientific). Seg-9 was amplified by polymerase chain reaction (PCR) using Seg-9 specific primers (FP CTCATGTCTTCGGCATTACTC and RP GCAAGCCCCTATCTACAGTAAATAAG) and GoTaq® G2 DNA Polymerase (Promega). Amplicons were sequenced using the ABI PRISM BigDye Terminator Cycle Sequencing kit v3.1 (Applied Biosystems) and the Applied Biosystems 3500xl genetic analyser (Life Technologies). Raw data was analysed using BioEdit [35] and aligned using MAFFT [36]. Amino acid sequences were aligned using CLC Main Workbench 8 (Qiagen Bioinformatics). The 3D structures were predicted using I-TASSER. The structural models predicted by I-TASSER were aligned with proteins in the protein data bank using TM-align to determine the structural analogs of each NS4 type. A TM-score >0.5 and C-score [-2; 5] was used to determine the confidence level of each prediction [37, 38].

Antibodies

For identification of AHSV proteins, rabbit anti-NS4 (Genscript) [21], and rabbit anti-NS2 [16] sera were available. Rabbit anti-NS1 was produced against a purified baculovirus expressed AHSV NS1 protein. An additional anti-NS4 antibody (batch E3F) was produced against a bacterially expressed and purified full-length AHSV NS4-II protein. Both anti-NS4 E3F and anti-NS1 were produced in rabbits

at the animal facilities of Deltamune (Pty) Ltd with Ethic Approval number O-15–17. Nuclear compartments were identified using mouse monoclonal anti-serine/arginine-rich splicing factor 2 (SRSF2) antibody (Merck; SAB4200725), mouse monoclonal anti-PML antibody (Santa Cruz; sc-966) and mouse anti-coilin antibody (Santa Cruz; sc-55594). Alexa Fluor™ 488 goat anti-rabbit (Invitrogen; A-11034) and Alexa Flour™ 594 goat anti-mouse (Invitrogen; A-11005) secondary antibodies were used for confocal laser scanning microscopy (CLSM).

Generation of recombinant baculoviruses expressing NS4

The baculovirus expression system was utilised to express NS4 proteins. Two recombinant baculoviruses were available, Bac-Seg-9 [39] and Bac-eGFP (kind gift from Prof Jacques Theron, Department of Biochemistry, Genetics and Microbiology, University of Pretoria). Bac-Seg-9 contained the full AHSV-3 Seg-9 gene from which it expressed both VP6 and NLS-NS4-II from different reading frames; Bac-eGFP expressed the eGFP protein. Additional recombinant baculoviruses (Table 2) were constructed according to the protocols in the Bac-to-Bac® Baculovirus Expression System (Invitrogen) manual. Briefly, the ORFs of NS4-I, NS4-II or NLS-NS4-II were PCR amplified using the primers as listed in Table 1 and cloned into the pFastBac1 (pFB) vector using BamHI and HindIII restriction sites to generate pFB-NS4-I, pFB-NS4-II and pFB-NLS-NS4-II. To allow expression of NS4-I and eGFP with an additional N-terminal NLS, In-Fusion cloning was used. The pFB vector plus the NLS sequence was PCR amplified from pFB-NLS-NS4-II to generate the pFB-NLS vector backbone, and joined to the PCR amplified NS4-I and eGFP inserts using an In-Fusion® HD Cloning Kit (Takara bio) to generate plasmids pFB-NLS-NS4-I and pFB-NLS-eGFP. Primers used to generate the vector backbone and inserts for the In-Fusion cloning contained 15 bp complementary overhangs (underlined). Sf9 cell monolayers were infected with recombinant baculovirus at an MOI of 1 – 5 and harvested or fixed at 24 – 72 hours post infection (hpi) for CLSM or Western blot.

Transient mammalian expression of AHSV NS4 or NS2

The NS4 gene sequence of AHSV-3 Field (Genbank KP009647) codon-optimised for Chinese hamster ovary cells, and the NS4 gene followed by the eGFP coding sequence, were synthesised and cloned by Genscript corporation into an expression plasmid phCMVdream (a kind gift from Piet van Rijn) to generate phCMV-NS4-II and phCMV-NS4-eGFP. A Glutathione S-transferase (GST) tag coding sequence was cloned downstream of the 3’ end of eGFP in phCMV-NS4-eGFP using the In-Fusion® HD Cloning Kit (ClonTech). GST specific primers (FP ATGGATGAACTGTATAAATCCCCTATACTAGGTTATTGG and RP GCTTTATTTACTAT GAGACGTCATTTTGGAGGATGGTCGC) and vector (phCMV-NS4-eGFP) specific primers (FP CATAGTAAATA AAGCAATAGCATCAC and RP ATACAGTTCATCCATCCCCAGG) were

supplied by Whitehead Scientific. Recombinant vectors were transformed into Stellar™ cells and plasmids isolated using the GeneJET Plasmid midiprep Kit (Thermo Scientific). Codon optimised phCMV-NS2-eGFP was a kind gift from Litia Yssel (Department of Genetics, University of Pretoria).

BSR cells were grown as monolayers on sterile coverslips in a 24-well plate. The medium was replaced with optiMEM® when cells reached 70% confluency. Cells were transfected with 400 ng of DNA in LF2000. After 4 h at 37°C the medium was replaced with complete EMEM and cells were prepared for CLSM at 48 h post-transfection.

SDS-polyacrylamide gel electrophoresis (SDS-PAGE) and Western blot analysis

Virus-infected cell monolayers were harvested at the required time point and lysed with RIPA buffer (150 mM sodium chloride; 1.0% Triton X-100; 0.5% sodium deoxycholate; 0.1% SDS [sodium dodecyl sulfate]; 50 mM Tris, pH 8.0) and incubated on ice with shaking for 30 min. Protein samples were resolved by 15% SDS-PAGE. The gel was transferred to a Hybond C nitrocellulose membrane (Amersham), and incubated with the required antibody after blocking. Peroxidase-conjugated protein A was used for detection.

Immunofluorescence microscopy

Cells monolayers grown on sterile glass coverslips in a 24-well plate were infected with the required virus and incubated for 24 - 30 hpi. Cells were fixed with 4% paraformaldehyde for 30 min, permeabilised with 0.4% Triton-X100 in PBS for 10 min at room temperature (RT), blocked for 30 min in 5% blocking solution (5% skim milk powder in PBS) followed by primary antibody labelling overnight at 4°C. Cells were washed three times in wash buffer (0.5% Tween-20 in PBS) followed by incubation in secondary antibody diluted in 1% blocking solution for 1 h at RT. Cells were then washed three times in wash buffer and once in PBS. DAPI staining (10 μg/ml) (Roche) was performed by incubation for 10 min at RT. If no antibody was required, cells were immediately subject to DAPI staining after incubation with Triton-X100. Coverslips were washed once with PBS and mounted on a microscope glass slide using VECTASHIELD Mounting Medium (Vector Laboratories). Immunofluorescence was visualised using a Zeiss LSM880 confocal microscope with Airyscan detector for super resolution microscopy. Intensity plot fluorescence profiles to confirm colocalisation was generated using Zeiss ZEN software.

Quantitative and statistical analysis

Individual cells were selected, and the perimeter of the entire cell or only the nucleus was delineated using Image J software. The fluorescent intensity and area values of either total cell (cytoplasmic plus

nuclear) or only nuclear were then determined by the software. In each image field, an uninfected cell was used and its cytoplasmic and nuclear fluorescent intensities used as the background value. The following formulas were used to calculate the cytoplasmic or nuclear fluorescent percentages.

$$\text{Cytoplasmic \%} = \frac{(\text{Total cell intensity} - \text{nuclear intensity})}{(\text{Total cell area} - \text{nuclear area})} - \frac{\text{Cytoplasmic background intensity}}{\text{Cytoplasmic background area}} \text{ x } 100$$

$$\text{Nuclear \%} = \frac{\text{Nuclear intensity}}{\text{Nuclear area}} - \frac{\text{Nuclear background intensity}}{\text{Nuclear background area}} \text{ x } 100$$

The significance was measured by one-way ANOVA followed by a Dunnett's T3 test using SPSS. The level of significance was $p<0.05$.

5. Results

Every AHSV strain expresses one of the NS4 types

In the first study done on AHSV NS4 the presence of an NS4 ORF was detected in Seg-9 of 26 AHSV isolates, however expression of the NS4 protein was only investigated for four strains [21]. We therefore analysed the NS4 gene sequences and NS4 protein production for all nine AHSV reference strains, and for recent Southern African field strain isolates representing each of the nine serotypes (Table 1). BSR-T7 cells were infected with these 18 AHSV strains, and dsRNA extracted after manifestation of full CPE. Sequencing of PCR amplicons of Seg-9 confirmed that all strains contained an NS4 ORF in a different reading frame to the VP6 ORF. Each virus encoded one of the two types of NS4 (Suppl. Fig. 1), i.e. either the 144 aa NS4-I protein or the slightly larger 154 aa NS4-II protein. One reference (AHSV-3 Ref) and one field (AHSV-8 Field) strain each encoded a variant of NS4-II (169 aa) with 15 additional N-terminal residues MGRRRTRVKRKRTKY containing a typical NLS sequence (underlined), therefore these proteins were termed NLS-NS4-II. The sizes and relative positions of the different NS4 ORFs on Seg-9 are depicted in Fig. 1a. Amino acid sequences from different strains representing each NS4 type were aligned (Fig. 1b), showing that the C-terminal region of all NS4 proteins is highly conserved. 3D structural modelling for all NS4 types using I-TASSER (Fig. 1c) predicted six or seven α-helices separated by short coiled regions for all three proteins, folding into an elongated shape. The predicted 3D model of all NS4 types obtained a good TM-score, however only NS4-II had a C score higher than 1.5 which represents a model of good quality. When aligning these 3D models with all structures in the protein data bank (Suppl. Table 1-3), the only viral protein identified

as a potential structural analog for NS4-II was the immediate-early 1 protein (IE1) of a primate cytomegalovirus (macacine herpesvirus 3).

Following confirmation of the presence of the NS4 ORFs, NS4 protein expression was investigated. When cell lysates from infected BSR-T7 cells were subjected to Western blot using anti-NS4 serum, NS4 synthesis was successfully detected for all AHSV strains (Fig. 2). Corresponding to the sequence predictions, six strains (AHSV-4, -6 Ref, AHSV-3, -4, -5, -7 Field) expressed the ±20 kDa NS4-I protein. Ten strains (AHSV-1, -2, -5, -7, -8, -9 Ref and AHSV-1, -2, -6, -9 Field) displayed a band of ±23 kDa corresponding to the size expected for NS4-II. For the two strains expressing NLS-NS4-II (AHSV-3 Ref and AHSV-8 Field) two protein bands of ±30 kDa and ±23 kDa respectively were detected with equal strength. The larger 30 kDa band represents the full-length NLS-NS4-II protein, with the smaller protein likely resulting from downstream translation initiation from the in-frame NS4-II start codon based on the predicted size of NS4-II.

As AHSV also replicates in its insect vector the *Culicoides* biting midge, we aimed to confirm the expression of NS4 in insect cells. Despite numerous attempts, we were never able to detect any NS4 protein in AHSV-infected KC cells (*Culicoides* cell line) or C6/36 cells (mosquito cell line) either by immunoblot or by confocal microscopy (results not shown). We used all AHSV strains at our disposal, and four different sets of anti-NS4 sera, but detection remained unsuccessful. Conditions utilised allowed clear identification of NS4 controls in mammalian cells, and strong positive signals of other virus proteins (e.g. VP7 and NS3) confirming viral infection and protein expression in insect cells. At this stage it is therefore still not clear as to whether or not NS4 is expressed in insect cells following AHSV infection.

Each NS4 type displays a unique intracellular distribution profile

Next, we assessed the intracellular localisation of NS4 following its expression in mammalian cells. BSR-T7 cells were infected with each AHSV strain, and prepared for CLSM at 24 hpi by fixing and subsequent labelling with anti-NS4 serum (Fig. 3a). In the case of all strains expressing NS4-I, the protein showed an essentially homogeneous distribution throughout the cell, however the NS4 signal was stronger in the nucleus compared to that of the cytoplasm. For strains expressing NS4-II the protein also distributed homogenously throughout the cell, however here NS4 was brighter in the cytoplasm than the nucleus. To confirm these observations, quantitative analyses were performed on CLSM images for least 40 cells per sample (from a minimum of two biological repeats), and average values of nuclear to cytoplasmic distribution ratio for NS4 were calculated for each strain. For NS4-I between

52-67% of the NS4 signal was nuclear, while for NS4-II the nuclear component represented 26-46% of the protein's distribution. In cells infected with AHSV-3 Ref or AHSV-8 Field, expressing NLS-NS4-II, the protein showed a bright homogeneous cytoplasmic fluorescence plus distinct punctate foci in the nucleus. The average nuclear or cytoplasmic distribution for each type of NS4 (Fig. 3b) was statistically significantly different from that of all other types. AHSV NS4 can therefore be described as a nucleocytoplasmic protein, localising to the nucleus and the cytoplasm.

NS4 expressed in the absence of other AHSV proteins shows the same subcellular localisation pattern as observed during AHSV infection

The bi-directional transport of proteins between the cytoplasm and nucleus of a cell facilitates the regulation of multiple and diverse cellular processes. This transport occurs exclusively though the nuclear pore complexes (NPC). While small molecules of 50-60 kDa or less than 10 nm in diameter can diffuse passively, most proteins are actively transported across the NPC by energy driven carrier-mediated transport [40]. Additionally the subcellular distribution of a protein can be influenced by the presence of nuclear localisation signals (NLSs) and/or nuclear export signal (NESs). It is not known whether NS4's presence in the nucleus is related to a specific biological function, and whether it is actively transported there or diffuses in as a result of its small size.

To investigate this we constructed expression plasmids for transient expression of NS4-II and eGFP, plus the fusion proteins NS4-II-eGFP, NLS-NS4-II-eGFP, and NS4-II-eGFP-GST, and transfected them into mammalian cells. NS4 distribution was visualised by immunolabelling (Fig. 4a) or autofluorescence (Fig. 4b) and confocal microscopy. NS4-II (±23 kDa), eGFP (±27 kDa) and NS4-II-eGFP (±46 kDa) showed a homogenous distribution in the nucleus and the cytoplasm. NLS-NS4-II-eGFP (±48 kDa) had a stronger cytoplasm fluorescence with punctate foci observed in some nuclei, and NS4-II-eGFP-GST (±70 kDa) had a homogenous distribution in the cytoplasm but no or very low fluorescence in the nucleus. This confirmed the NS4-II distribution profiles observed in AHSV-infected cells, and indicated that the NLS sequence could be responsible for the formation of nuclear foci. As the largest NS4 fusion protein containing a C-teminal GST tag (NS4-eGFP-GST) with a molecular weight exceeding the 60 kDa limit for diffusion was excluded from the nucleus, the normal mechanism whereby the small native NS4 localises to the nucleus is therefore probably via passive diffusion.

To further confirm that the intracellular localisation of NS4 was inherent to the protein and not influenced by the presence of other AHSV proteins during the viral infection cycle, we utilised the baculovirus expression system. We had a recombinant baculovirus available that contained the full-

length AHSV-3 Seg-9 [41] and expressed both VP6 and NLS-NS4-II. In addition we generated recombinant baculoviruses that expressed the ORFs of NS4-I, NS4-II and NLS-NS4-II, plus novel fusions of the NLS sequence to the N-terminal of NS4-I and eGFP to generate NLS-NS4-I and NLS-eGFP. A schematic representation of all recombinant baculoviruses are shown in Fig. 5a. Western blot (Fig. 5b) confirmed the synthesis of protein products within the expected size range. When infected cells were analysed by immunofluorescence and CLSM (Fig. 6), it was clear that the intracellular distribution of NS4 expressed from the recombinant baculoviruses in insect cells remained essentially the same to that observed for the cognate NS4 type in AHSV-infected mammalian cells. NS4-I was homogenous throughout the cell but showed stronger nuclear fluorescence, NS4-II was homogenous but more cytoplasmic, and NLS-NS4-II, the NLS-NS4-II expressed from Bac-Seg-9, NLS-NS4-I and NLS-GFP had distinct nuclear foci plus a homogenous cytoplasmic distribution. Collectively these results show that the intracellular distribution is different for each type of NS4, and this is not affected by the presence or absence of other AHSV proteins. The NLS sequence confers a unique distribution on a subset of the proteins and allows aggregation into small punctate nuclear foci.

NS4 is absent from Cajal bodies but localises to PML-nuclear bodies

For RNA viruses replicating in the cytoplasm, specific viral proteins that enter the nucleus often interfere with cellular factors involved in signalling related to the innate immune system [42]. As AHSV NS4 shows a nucleocytoplasmic distribution, we set out to determine whether NS4 localises to any of three of the subnuclear compartments typically targeted by RNA viruses to mediate immune suppression or interfere with host processes, i.e. Cajal bodies, PML-nuclear bodies (PML-NBs) or nuclear speckles. We selected one AHSV strain that represents each type of NS4 for these analyses, namely AHSV-4 Field (NS4-I), AHSV-1 Field (NS4-II) and AHSV-8 Field (NLS-NS4-II). To enable us to compare the effect of a virus with and without NS4 we also included two recombinant AHSV strains rescued by reverse genetics, namely rAHSV-5 (NS4-II) and rAHSV-5ΔNS4 which is NS4 deficient.

Firstly, we investigated if AHSV NS4 localised to Cajal bodies. Cajal bodies may play a crucial role in viral pathogenesis due to their close interaction with the nucleolus. It has been shown that plant viruses reorganise Cajal bodies during viral infection and use them as a pathway to localise to the nucleolus [43, 44]. HeLa cells were infected with the selected AHSV strains and cells were prepared for CLSM at 24 hpi by fixation and dual labelling for NS4 in combination with a primary antibody directed against coilin, a marker for Cajal bodies (Fig. 7). Each type of NS4 displayed its distinct intracellular localisation pattern, however as can be seen from the graphs NS4 did not specifically colocalise with

coilin. In cells infected with AHSV-8 Field, sometimes a number of the NLS-NS4-II nuclear foci were in very close proximity to the punctate Cajal bodies with some overlap at their perimeters. This was however not always the case, and in other cells (not shown) there was no colocalisation between NS4 foci and the Cajal bodies.

We next investigated whether AHSV NS4 colocalised with PML-NBs, which are well known nuclear bodies involved in antiviral responses [45]. AHSV-infected cells were dual labelled with anti-NS4 and anti-PML antibodies (Fig. 8). Both NS4-I expressed from AHSV-4 Field, and NS4-II expressed from AHSV-1 Field and rAHSV-5, colocalised with the PML-NBs in the nucleus. Large and small nuclear foci could be distinguished in cells infected with AHSV-8 Field, only some foci colocalised with PML-NBs.

In mock-infected cells, or cells infected with any of the wild-type AHSV strains, the PML-NBs were essentially spherical as expected [46]. Interestingly, the morphology of the PML-NBs changed upon rAHSV-5ΔNS4 infection and became distinctly elongated. As this resembled the distribution profile we had previously observed when visualising AHSV NS1 in infected cells, we dual labelled for NS1 and PML (Fig. 9). Non-structural protein NS1 forms characteristic tubule-like structures of which the bulk are present in the cytoplasm, however the presence of some NS1 tubules in the nucleus has been reported [18, 47]. As expected, strong labelling of the aggregates of NS1 tubules could be clearly distinguished in the cytoplasm, with some nuclear labelling of NS1 tubule bundles. In the nucleus the terminal regions of the NS1 structures of AHSV-1 Field, AHSV-4 Field, AHSV-8 Field and rAHSV-5 colocalised with PML at the perimeters of the PML-NBs. With rAHSV-5ΔNS4 infection the colocalisation was more extensive, with the majority of the NS1 signal colocalising with the elongated PML-NBs.

The SRSF2 protein of nuclear speckles localises to AHSV viral inclusion bodies in the cytoplasm

Lastly, the presence of AHSV NS4 in nuclear speckles was investigated. Nuclear speckles, also called splicing speckles, are nuclear bodies that are key gene expression regulators that act primarily via mRNA splicing regulation [48]. Mock- or AHSV-infected BSR-T7 cells were fixed and labelled with anti-SRSF2, a marker of nuclear speckles (Fig. 10). In mock-infected cells the SRSF2 protein (previously known as SC35) localised to discrete intranuclear speckles. Contrary to expectations, in all AHSV-infected cells (including rAHSV-5ΔNS4) SRSF2 was completely absent from the nucleus and displayed strong punctate labelling in the cytoplasm. SRSF2 did not colocalise with any of the NS4 proteins (not shown). The size and distribution of the cytoplasmic SRSF2 foci were reminiscent of the

morphology of AHSV viral inclusion bodies (VIBs). VIBs are cytoplasmic aggregates of non-structural protein NS2 that act as viral factories where genome replication and progeny virion assembly take place. We investigated this further by infecting BSR-T7 cells with AHSV, and dual-labelling with anti-SRSF2 and anti-NS2 (Fig. 11). In most cases there was a full overlap between the signals for these two proteins.

To further confirm these results, we asked whether the relocation of SRSF2 was due exclusively to the presence of NS2 or as a result of the viral infection. We therefore transfected BSR cells with a plasmid expressing either NS2 (phCMV-NS2-eGFP) or eGFP (pCMV-eGFP) as control, and labelled with anti-SRSF2 (Fig. 12). Expression of eGFP resulted in its distribution throughout the cytoplasm and nucleus, while SRSF2 labelling was restricted to the nucleus in a pattern similar to mock-transfected cells. Transient expression of NS2 resulted in the formation of VIB-like cytoplasmic foci and colocalisation of SRSF2 with these foci. This confirmed that the translocation of SRSF2 required only NS2 and was independent of the expression of other AHSV proteins including NS4.

6. Discussion

While it has been known for more than a century that AHS is caused by a virus, the non-structural protein NS4 was only identified nine years ago [21, 22]. The specific role of AHSV NS4 in viral pathogenesis and the AHSV life cycle still remains largely unknown. For this study we aimed to characterise NS4 across all AHSV serotypes. We identified a novel co-localisation of NS4 with PML-NBs, nuclear bodies which amongst other functions are involved in innate immunity. Unexpectedly we also observed that two of the other AHSV non-structural proteins, NS1 and NS2, potentially interact with specific nuclear compartments or usurp nuclear proteins during the AHSV life cycle.

Our assessment of all nine AHSV reference strains plus a field isolate of each serotype confirmed that an NS4 open reading frame (ORF) was present in all Seg-9 gene sequences. The ORF encoded either NS4-I or the slightly longer NS4-II or NLS-NS4-II, with each of these variants displaying distinct size bands on a Western blot. Despite numerous attempts, we were not able to detect any NS4 expression in AHSV-infected insect cells. This is in contrast to NS4 of BTV [22], and our own results of baculovirus expression of AHSV NS4. Our expression level of NS4 was however significantly lower than typically expected from this system, where the foreign gene is placed under control of a strong late baculovirus promoter. We were unable to detect NS4 in Sf9 cells by Coomassie staining, and had to rely on immunoblots to confirm its presence. One of the major differences between insect and mammalian cells is that no CPE is observed in insect cells following AHSV infection [47]. In the case of the tick-borne orbivirus St Croix River virus (SCRV), the NS4 ORF is interrupted by a stop codon and hence non-

functional [22, 49]. Replication of SCRV can only occur in insect cells and not mammalian cells, therefore the orbivirus NS4 may play an important role in enhancing replication in specific cell types. Whether there is any cell-specific regulation of the levels of AHSV NS4 expression remains to be investigated.

We observed differences in the intracellular localisation profiles of the AHSV NS4 variants. All types of NS4 showed a homogenous cytoplasmic distribution, plus a nuclear presence. However, NS4-I had a higher nuclear than cytoplasmic signal, NS4-II had a higher cytoplasmic than nuclear signal and NLS-NS4-II had distinct punctate foci in the nucleus. The nuclear localisation of AHSV NS4 is intriguing, as AHSV replicates exclusively in the cytoplasm. For DNA viruses that replicate in the nucleus, efficient nuclear entry of many viral components is crucial. However recent evidence shows that various cytoplasmic replicating RNA viruses also utilise nucleocytoplasmic trafficking of viral proteins to carry out specific roles in viral replication or pathogenesis, and/or modulate the host cell cycle or innate immune response [42, 50]. Examples include the avian reovirus nonstructural protein p17 [51], the mammalian reovirus non-structural protein σ1s [52], Dengue virus NS5 proteins [53, 54] and the coronavirus nucleocapsid protein [55]. West Nile Virus NS5 shuttles between the nucleus and the cytoplasm, and inhibition of the nuclear import of NS5 causes a decrease in virus replication [54] . Chemical inhibition of the pathways used by these nuclear proteins can be used as a drug target to decrease viral replication [54, 56].

AHSV NS4 could passively diffuse through the nuclear pore complex as a result of its small size, or it could be actively trafficked in and/or out of the nucleus. Nuclear trafficking relies on the presence of specific NLSs or nuclear export signals (NESs) in the target protein, that interact with cellular importin (IMP) or exportin (EXP) proteins of the karyopherin-ß family [25, 57]. NLS-NS4-II contains a classical monopartite basic NLS which may mediate its nuclear entry, however the bulk of AHSV strains express a NS4 protein lacking this NLS that still localise to the nucleus. When we increased the size of NS4-II to exceed the passive diffusion limit of 60 kDa by adding a GST tag, it was excluded from the nucleus and localised exclusively to the cytoplasm, indicating that its nuclear entry is probably via diffusion. The NLS-NS4-II protein did however show a unique phenotype, which was accumulation of a portion of the protein into distinct nuclear foci. We fused this 17 residue NLS peptide to the N-termini of NS4-I and eGFP and expressed these recombinant proteins via the baculovirus system. Both NLS-eGFP and NLS-NS4-I formed punctate foci in the nucleus of Sf9 cells, confirming that the NLS sequence is required for foci formation in the nucleus. The mechanism underlying this observation is currently unknown.

NESs typically comprise three to four hydrophobic residues interspersed with non-hydrophobic residues, which are recognised by exportins such as EXP-1 (CRM-1) [58, 59]. Sequence analysis (not shown) indicated that NS4-I contains a stronger potential NES in the conserved C-terminal region of the protein than NS4-II. This seems counterintuitive, as NS4-I has a higher nuclear to cytoplasmic ratio than NS4-II. However, NESs can be masked / unmasked either by homo-dimerisation of the cargo protein, or interaction of the cargo protein with other cellular proteins, allowing tight regulation of export. The human immunodeficiency virus type 1 Rev protein is a classical viral example of this phenomenon, where Rev masks its own NES to regulate its trafficking [60]. We will need to conduct further investigations, e.g. by inhibition of the exporter CRM-1 or modification of the NES sequences, to assess whether nuclear export of NS4 is regulated and if this could contribute to the observed difference in nuclear to cytoplasmic ratio of NS4-I and NS4-II.

A eukaryotic nucleus contains distinct chromatin territories, mainly consisting of DNA-protein complexes, plus several interchromosomal compartments. The best characterised of these subnuclear structures include the nucleolus, nuclear (or splicing) speckles, Cajal bodies and promyelocytic leukaemia nuclear bodies (PML-NBs), which all support different nuclear molecular activities. Components of these nuclear compartments are known to play a role in the replication cycles of multiple viruses [28, 61]. Based on this, we aimed to investigate whether AHSV NS4 localises to or disrupts any of these nuclear compartments. We have shown previously that AHSV NS4, in contrast to BTV NS4 [22], is not present in the nucleolus [21]. In this study we confirmed that NS4 also does not colocalise with coilin, a component of Cajal bodies.

We showed here that all the different forms of AHSV NS4 colocalise with PML-NBs. PML-NBs consist of numerous cellular proteins, which accumulate as distinct foci in the nucleus, with the protein PML acting as the key organiser of the PML-NB structure [62]. PML-NBs play multiple roles in the cell such as transcriptional regulation, epigenetics and apoptosis [63], but importantly there is more data emerging that PML are components of the antiviral defense against a variety of DNA and RNA viruses (reviewed in [64]). $PML^{-/-}$ mice or cell lines have been shown to be more susceptible to infection by a range of different viruses, e.g. vesicular stomatitis virus [65], human cytomegalovirus (HCMV) [66], rabies virus [67] and HIV-1 [45]. PML-NBs can inhibit viral replication by diverse mechanism, either via the intrinsic antiviral activity of specific PML components or by activation of innate immune responses. PML has been shown to act both as a positive regulator of IFN-γ signalling [68] and of IFN-β synthesis [45]. A number of the PML-NB proteins are themselves upregulated in response to IFN. Hence many viruses have evolved mechanisms to evade the antiviral function of PML-NBs. These can

include either antagonistic proteins that target individual PML-NB components, or activities that affect the integrity of the whole cellular structure [28, 64].

When we predicted 3D structural models for NS4 and matched these to all structures in the protein databank (PDB), the only viral protein predicted as a structural analog for NS4-II was the cytomegalovirus immediate-early protein IE1 (PDB 4WID) [69]. HCMV IE1 has long been known to act as an antagonist of the immune defences that target HCMV immediately after infection [69]. The globular core of IE1 interacts with PML via coiled-coil domains [69], and this interaction antagonises the PML-mediated intrinsic immunity against HCMV and affects the function of PML in innate immune signalling [70, 71]. The colocalisation of AHSV NS4 with PML-NBs, plus its structural similarity to IE1, indicates a potential role for NS4 in counteracting the innate immune response. Future work should include measuring the replication kinetics of AHSV in PML knockout cells, and investigating the interaction of NS4 with specific isoforms of PML. Whether our observed interaction of NS1 with PML-NBs, enhanced by the absence of NS4, could provide an additional mechanism whereby AHSV interferes with host immunity also requires future investigation.

We provided evidence that AHSV infection disrupts another nuclear compartment, by relocating the SRSF2 (SC35) component of nuclear speckles. When we started the investigation we presumed that NS4 would be the only AHSV protein to be associated with nuclear proteins or processes, however in this case it seems as though NS4 plays no role and NS2 is exclusively responsible for the translocation to or retention of SRSF2 in the cytoplasm and specifically within the VIBs. The main role of nuclear speckles is storage, assembly or recycling of eukaryotic splicing factors used for host transcript processing [72], but splicing factors like SRSF2 can also regulate viral mRNA splicing [73]. AHSV RNAs are not spliced, however sequestering SRSF2 to the VIBs could provide a mechanism for AHSV to deplete host splicing resources and alter host mRNA maturation as seen for human rhinovirus [74]. Inhibiting host processes in this way can contribute to creating a cellular environment that favours viral replication. The µ2 protein of reovirus strain T1L localises to nuclear speckles by complexing with SRSF2, and thereby alters the splicing of host gene transcripts [50]. Reovirus µ2 is a minor capsid protein, which in addition to its role in antagonising SRSF2 also localises to and determines the morphology of the cytoplasmic viral factories [75] and represses IFN-ß signalling [76], illustrating the pleiotropy common to many viral proteins. Reovirus viral factories (VFs) and rotavirus viroplasms are the functional equivalents of orbivirus VIBs. These dense cytoplasmic matrices were traditionally considered to only act as sites for viral genome replication and assembly of progeny virions [77-79]. Recent evidence however indicates that reovirus VFs can also act in recruiting host translational machinery [80] and modulate stress granule protein localisation [81], while rotavirus infection induces

cytoplasmic re-localization of a large number of nuclear RNA-binding proteins of which the majority associate with viroplasms [82, 83]. We present evidence that orbivirus VIBs can also contribute to interfering with host processes by sequestering SRSF2. Further work will focus on elucidating how this impacts nuclear speckle structure, host transcription and advancing the AHSV life cycle.

Many cytoplasmic viruses encode nuclear proteins that suppress the immune response, these are often major determinants of viral pathogenesis and can be important targets in vaccine development [84-86]. This study confirmed the variability and strain-specific differences of AHSV NS4, in contrast to BTV where only one type of NS4 exists. We concluded that AHSV NS4 can play a role in the immune response by localising to PML-NBs. The functional importance of the different forms of NS4 (NS4-I versus NS4-II/NLS-NS4-II) still remains unknown, but it may relate to differences in the immune response upon AHSV infection with a virus expressing a specific NS4. Functional analyses of the different forms of NS4 would need to be conducted to assess this. This could however also be impacted by other viral proteins. AHSV virulence is complex and multifactorial, and as for BTV probably involves at least the capsid proteins VP2 and VP5 and non-structural protein NS3 [87, 88]. This is the first report implicating a role for NS1 in the nucleus via interaction with PML-NBs, which appears to be enhanced in the absence of NS4. This is also the first study to indicate that NS2 can recruit host nuclear proteins into VIBs to potentially subvert host processes to benefit the virus. The present study lays the foundation for future explorations of the mechanisms and implications of these interactions. If NS4 plays a central role in interfering with host immunity it could be an important AHSV virulence factor and a target for virus attenuation and vaccine development.

7. Author statements

7.1 Authors and contributors

1. Shareen Boughan

Conceptualization; Data curation; Formal Analysis; Investigation; Methodology; Project administration; Visualisation; Writing – original draft

2. Abraham Christiaan Potgieter

Conceptualization; Funding acquisition; Methodology; Project administration; Resources; Supervision; Validation; Writing – review and editing

3. Vida van Staden

Conceptualization; Funding acquisition; Methodology; Project administration; Resources; Supervision; Validation; Writing – review and editing

7.2 Conflicts of interest

There are no conflicts of interest to disclose.

7.3 Funding information

This work was supported by the University of Pretoria Institutional Research Theme, South Africa (Grant A0V004), the Poliomyelitis Research Foundation, South Africa (Grants 13/21 and 16/26) and Deltamune (Pty) Ltd, South Africa. Graduate bursary support was received from the National Research Foundation of South Africa, South Africa (Grant number 101518), the Poliomyelitis Research Foundation, South Africa (Grants 19/72 and 14/35) and the University of Pretoria, South Africa.

7.4 Ethical approval

Ethic Approval number O-15–17

7.5 Consent for publication

[If your article includes details, images, or videos relating to an individual person, you will need to have evidence of written informed consent for the publication of these details. Consent for publication must be obtained from the person, or their parent or legal guardian in the case of children under 18. If the person has died, consent for publication must be obtained from their next of kin.]

7.6 Acknowledgements

We would like to thank Phillip Wege for his assistance with cell culture, Sunette Vos for the synthesis of two recombinant baculoviruses and Carlo de Sá for his assistance with the colocalisation intensity graphs. We would also like to thank Eudri Venter, Erna van Wilpe and Alan Hall from the Laboratory for Microscopy and Microanalysis at the University of Pretoria for their assistance with confocal laser scanning microscopy.

8. References

1. **Theiler A**. African Horse Sickness (Pestis equorum). *Union S Africa Dept Agric, Pretoria, Sci Bull* 1921(19):30
2. **M'Fadyean J**. African horse-sickness. *J Comp Pathol* 1900;13:1-20.doi: https://doi.org/10.1016/S0368-1742(00)80001-6
3. **McIntosh BM**. Immunological types of horsesickness virus and their significance in immunization. *Onderstepoort J Vet Res* 1958;27(4):465-538
4. **Howell PG**. The isolation and identification of further antigenic types of African horsesickness virus. *Onderstepoort J Vet Res* 1962;29:139-149
5. **Calisher CH, Mertens PP**. Taxonomy of African horse sickness viruses. *Arch Virol Suppl* 1998;14:3-11.doi: 10.1007/978-3-7091-6823-3_1
6. **Meiswinkel R, Paweska JT**. Evidence for a new field Culicoides vector of African horse sickness in South Africa. *Prev Vet Med* 2003;60(3):243-253.doi: 10.1016/s0167-5877(02)00231-3
7. **Alexander RA, Neitz WO, Du Toit PJ**. Horsesickness: Immunization of horses and mules in the field during the season 1934-1935 with a description of the technique of preparation of polyvalent mouse neurotropic vaccine. *Onderstepoort J Vet Res* 1936;7

8. **Mirchamsy H, Taslimi H**. Immunization Against African Horse Sickness with Tissue-Culture-Adapted Neurotropic Viruses. *Br Vet J* 1964;120(10):481-486.doi: https://doi.org/10.1016/S0007-1935(17)41556-9
9. **Weyer CT, Grewar JD, Burger P, Rossouw E, Lourens C et al.** African Horse Sickness Caused by Genome Reassortment and Reversion to Virulence of Live, Attenuated Vaccine Viruses, South Africa, 2004-2014. *Emerging infectious diseases* 2016;22(12):2087-2096.doi: 10.3201/eid2212.160718
10. **Burrage TG, Laegreid WW**. African horsesickness: pathogenesis and immunity. *Comp Immunol Microbiol Infect Dis* 1994;17(3-4):275-285.doi: 10.1016/0147-9571(94)90047-7
11. **Oellermann RA, Els HJ, Erasmus BJ**. Characterization of African horsesiekness virus. *Archiv für die gesamte Virusforschung* 1970;29(2-3):163-174.doi: 10.1007/BF01249302
12. **Roy P, Mertens PP, Casal I**. African horse sickness virus structure. *Comp Immunol Microbiol Infect Dis* 1994;17(3-4):243-273.doi: 10.1016/0147-9571(94)90046-9
13. **Maree FF, Huismans H**. Characterization of tubular structures composed of nonstructural protein NS1 of African horsesickness virus expressed in insect cells. *J Gen Virol* 1997;78 (Pt 5):1077-1082.doi: 10.1099/0022-1317-78-5-1077
14. **Boyce M, Celma CC, Roy P**. Bluetongue virus non-structural protein 1 is a positive regulator of viral protein synthesis. *Virol J* 2012;9:178.doi: 10.1186/1743-422x-9-178
15. **Kerviel A, Ge P, Lai M, Jih J, Boyce M et al.** Atomic structure of the translation regulatory protein NS1 of bluetongue virus. *Nat Microbiol* 2019;4(5):837-845.doi: 10.1038/s41564-019-0369-x
16. **Uitenweerde JM, Theron J, Stoltz MA, Huismans H**. The multimeric nonstructural NS2 proteins of bluetongue virus, African horsesickness virus, and epizootic hemorrhagic disease virus differ in their single-stranded RNA-binding ability. *Virology* 1995;209(2):624-632.doi: 10.1006/viro.1995.1294
17. **Stoltz MA, van der Merwe CF, Coetzee J, Huismans H**. Subcellular localization of the nonstructural protein NS3 of African horsesickness virus. *Onderstepoort J Vet Res* 1996;63(1):57-61
18. **Ferreira-Venter L, Venter E, Theron J, van Staden V**. Targeted mutational analysis to unravel the complexity of African horse sickness virus NS3 function in mammalian cells. *Virology* 2019;531:149-161.doi: 10.1016/j.virol.2019.03.005
19. **van de Water SG, van Gennip RG, Potgieter CA, Wright IM, van Rijn PA**. VP2 Exchange and NS3/NS3a Deletion in African Horse Sickness Virus (AHSV) in Development of Disabled Infectious Single Animal Vaccine Candidates for AHSV. *J Virol* 2015;89(17):8764-8772.doi: 10.1128/JVI.01052-15
20. **Firth AE**. Bioinformatic analysis suggests that the Orbivirus VP6 cistron encodes an overlapping gene. *Virol J* 2008;5:48.doi: 10.1186/1743-422x-5-48
21. **Zwart L, Potgieter CA, Clift SJ, van Staden V**. Characterising Non-Structural Protein NS4 of African Horse Sickness Virus. *PLoS One* 2015;10(4):e0124281.doi: 10.1371/journal.pone.0124281
22. **Belhouchet M, Mohd Jaafar F, Firth AE, Grimes JM, Mertens PP et al.** Detection of a fourth orbivirus non-structural protein. *PLoS One* 2011;6(10):e25697.doi: 10.1371/journal.pone.0025697
23. **Ratinier M, Caporale M, Golder M, Franzoni G, Allan K et al.** Identification and characterization of a novel non-structural protein of bluetongue virus. *PLoS Pathog* 2011;7(12):e1002477.doi: 10.1371/journal.ppat.1002477
24. **Kalderon D, Roberts BL, Richardson WD, Smith AE**. A short amino acid sequence able to specify nuclear location. *Cell* 1984;39(3 Pt 2):499-509.doi: 10.1016/0092-8674(84)90457-4

25. **Freitas N, Cunha C**. Mechanisms and signals for the nuclear import of proteins. *Curr Genomics* 2009;10(8):550-557.doi: 10.2174/138920209789503941
26. **Feldherr CM, Kallenbach E, Schultz N**. Movement of a karyophilic protein through the nuclear pores of oocytes. *J Cell Biol* 1984;99(6):2216-2222.doi: 10.1083/jcb.99.6.2216
27. **Ratinier M, Shaw AE, Barry G, Gu Q, Di Gialleonardo L et al.** Bluetongue Virus NS4 Protein Is an Interferon Antagonist and a Determinant of Virus Virulence. *J Virol* 2016;90(11):5427-5439.doi: 10.1128/jvi.00422-16
28. **Zakaryan H, Stamminger T**. Nuclear remodelling during viral infections. *Cell Microbiol* 2011;13(6):806-813.doi: 10.1111/j.1462-5822.2011.01596.x
29. **Buchholz UJ, Finke S, Conzelmann KK**. Generation of bovine respiratory syncytial virus (BRSV) from cDNA: BRSV NS2 is not essential for virus replication in tissue culture, and the human RSV leader region acts as a functional BRSV genome promoter. *J Virol* 1999;73(1):251-259
30. **Potgieter AC, Wright IM, van Dijk AA**. Consensus Sequence of 27 African Horse Sickness Virus Genomes from Viruses Collected over a 76-Year Period (1933 to 2009). *Genome Announc* 2015;3(5).doi: 10.1128/genomeA.00921-15
31. **Bachanek-Bankowska K, Maan S, Castillo-Olivares J, Manning NM, Maan NS et al.** Real time RT-PCR assays for detection and typing of African horse sickness virus. *PLoS One* 2014;9(4):e93758.doi: 10.1371/journal.pone.0093758
32. **van Rijn PA, Maris-Veldhuis MA, Potgieter CA, van Gennip RGP**. African horse sickness virus (AHSV) with a deletion of 77 amino acids in NS3/NS3a protein is not virulent and a safe promising AHS Disabled Infectious Single Animal (DISA) vaccine platform. *Vaccine* 2018;36(15):1925-1933.doi: 10.1016/j.vaccine.2018.03.003
33. **Potgieter AC, Wright IM, Erasmus BJ, inventors;** Live attenuated African horsesickness virus. South Africa patent WO 2016/071850. 2017 2017-10-11.
34. **Conradie AM, Stassen L, Huismans H, Potgieter CA, Theron J**. Establishment of different plasmid only-based reverse genetics systems for the recovery of African horse sickness virus. *Virology* 2016;499:144-155.doi: 10.1016/j.virol.2016.07.010
35. **Hall TA**. BIOEDIT: a user-friendly biological sequence alignment editor and analysis program for Windows 95/98/ NT. *Nucleic Acids Symp* 1999
36. **Katoh K, Standley DM**. MAFFT multiple sequence alignment software version 7: improvements in performance and usability. *Mol Biol Evol* 2013;30(4):772-780.doi: 10.1093/molbev/mst010
37. **Yang J, Zhang Y**. Protein Structure and Function Prediction Using I-TASSER. *Curr Protoc Bioinformatics* 2015;52:5.8.1-5.8.15.doi: 10.1002/0471250953.bi0508s52
38. **Zhang Y**. I-TASSER server for protein 3D structure prediction. *BMC Bioinformatics* 2008;9:40.doi: 10.1186/1471-2105-9-40
39. **Turnbull PJ, Cormack SB, Huismans H**. Characterization of the gene encoding core protein VP6 of two African horsesickness virus serotypes. *J Gen Virol* 1996;77 (Pt 7):1421-1423.doi: 10.1099/0022-1317-77-7-1421
40. **Allen TD, Cronshaw JM, Bagley S, Kiseleva E, Goldberg MW**. The nuclear pore complex: mediator of translocation between nucleus and cytoplasm. *J Cell Sci* 2000;113 (Pt 10):1651-1659
41. **de Waal PJ, Huismans H**. Characterization of the nucleic acid binding activity of inner core protein VP6 of African horse sickness virus. *Arch Virol* 2005;150(10):2037-2050.doi: 10.1007/s00705-005-0547-4
42. **Fulcher AJ, Jans DA**. Regulation of nucleocytoplasmic trafficking of viral proteins: an integral role in pathogenesis? *Biochim Biophys Acta* 2011;1813(12):2176-2190.doi: 10.1016/j.bbamcr.2011.03.019

43. **Kim SH, Ryabov EV, Kalinina NO, Rakitina DV, Gillespie T et al.** Cajal bodies and the nucleolus are required for a plant virus systemic infection. *Embo j* 2007;26(8):2169-2179.doi: 10.1038/sj.emboj.7601674
44. **Love AJ, Yu C, Petukhova NV, Kalinina NO, Chen J et al.** Cajal bodies and their role in plant stress and disease responses. *RNA Biol* 2017;14(6):779-790.doi: 10.1080/15476286.2016.1243650
45. **El Asmi F, Maroui MA, Dutrieux J, Blondel D, Nisole S et al.** Implication of PMLIV in both intrinsic and innate immunity. *PLoS Pathog* 2014;10(2):e1003975.doi: 10.1371/journal.ppat.1003975
46. **Lallemand-Breitenbach V, de The H**. PML nuclear bodies. *Cold Spring Harb Perspect Biol* 2010;2(5):a000661.doi: 10.1101/cshperspect.a000661
47. **Venter E, van der Merwe CF, Buys AV, Huismans H, van Staden V**. Comparative ultrastructural characterization of African horse sickness virus-infected mammalian and insect cells reveals a novel potential virus release mechanism from insect cells. *J Gen Virol* 2014;95(Pt 3):642-651.doi: 10.1099/vir.0.060400-0
48. **Galganski L, Urbanek MO, Krzyzosiak WJ**. Nuclear speckles: molecular organization, biological function and role in disease. *Nucleic Acids Res* 2017;45(18):10350-10368.doi: 10.1093/nar/gkx759
49. **Belhouchet M, Mohd Jaafar F, Tesh R, Grimes J, Maan S et al.** Complete sequence of Great Island virus and comparison with the T2 and outer-capsid proteins of Kemerovo, Lipovnik and Tribec viruses (genus Orbivirus, family Reoviridae). *J Gen Virol* 2010;91(Pt 12):2985-2993.doi: 10.1099/vir.0.024760-0
50. **Rivera-Serrano EE, Fritch EJ, Scholl EH, Sherry B**. A Cytoplasmic RNA Virus Alters the Function of the Cell Splicing Protein SRSF2. *J Virol* 2017;91(7).doi: 10.1128/jvi.02488-16
51. **Costas C, Martinez-Costas J, Bodelon G, Benavente J**. The second open reading frame of the avian reovirus S1 gene encodes a transcription-dependent and CRM1-independent nucleocytoplasmic shuttling protein. *J Virol* 2005;79(4):2141-2150.doi: 10.1128/JVI.79.4.2141-2150.2005
52. **Belli BA, Samuel CE**. Biosynthesis of reovirus-specified polypeptides: expression of reovirus S1-encoded sigma 1NS protein in transfected and infected cells as measured with serotype specific polyclonal antibody. *Virology* 1991;185(2):698-709.doi: 10.1016/0042-6822(91)90541-i
53. **Hannemann H, Sung PY, Chiu HC, Yousuf A, Bird J et al.** Serotype-specific differences in dengue virus non-structural protein 5 nuclear localization. *J Biol Chem* 2013;288(31):22621-22635.doi: 10.1074/jbc.M113.481382
54. **Lopez-Denman AJ, Russo A, Wagstaff KM, White PA, Jans DA et al.** Nucleocytoplasmic shuttling of the West Nile virus RNA-dependent RNA polymerase NS5 is critical to infection. *Cell Microbiol* 2018;20(8):e12848.doi: 10.1111/cmi.12848
55. **Cawood R, Harrison SM, Dove BK, Reed ML, Hiscox JA**. Cell cycle dependent nucleolar localization of the coronavirus nucleocapsid protein. *Cell Cycle* 2007;6(7):863-867.doi: 10.4161/cc.6.7.4032
56. **Audsley MD, Jans DA, Moseley GW**. Nucleocytoplasmic trafficking of Nipah virus W protein involves multiple discrete interactions with the nuclear import and export machinery. *Biochem Biophys Res Commun* 2016;479(3):429-433.doi: 10.1016/j.bbrc.2016.09.043
57. **Marfori M, Mynott A, Ellis JJ, Mehdi AM, Saunders NF et al.** Molecular basis for specificity of nuclear import and prediction of nuclear localization. *Biochim Biophys Acta* 2011;1813(9):1562-1577.doi: 10.1016/j.bbamcr.2010.10.013

58. **la Cour T, Kiemer L, Molgaard A, Gupta R, Skriver K et al.** Analysis and prediction of leucine-rich nuclear export signals. *Protein Eng Des Sel* 2004;17(6):527-536.doi: 10.1093/protein/gzh062
59. **Fung HY, Fu SC, Chook YM**. Nuclear export receptor CRM1 recognizes diverse conformations in nuclear export signals. *Elife* 2017;6.doi: 10.7554/eLife.23961
60. **Behrens RT, Aligeti M, Pocock GM, Higgins CA, Sherer NM**. Nuclear Export Signal Masking Regulates HIV-1 Rev Trafficking and Viral RNA Nuclear Export. *J Virol* 2017;91(3).doi: 10.1128/JVI.02107-16
61. **Mao YS, Zhang B, Spector DL**. Biogenesis and function of nuclear bodies. *Trends Genet* 2011;27(8):295-306.doi: 10.1016/j.tig.2011.05.006
62. **Negorev D, Maul GG**. Cellular proteins localized at and interacting within ND10/PML nuclear bodies/PODs suggest functions of a nuclear depot. *Oncogene* 2001;20(49):7234-7242.doi: 10.1038/sj.onc.1204764
63. **Krieghoff-Henning E, Hofmann TG**. Role of nuclear bodies in apoptosis signalling. *Biochim Biophys Acta* 2008;1783(11):2185-2194.doi: 10.1016/j.bbamcr.2008.07.002
64. **Scherer M, Stamminger T**. Emerging Role of PML Nuclear Bodies in Innate Immune Signaling. *J Virol* 2016;90(13):5850-5854.doi: 10.1128/JVI.01979-15
65. **Bonilla WV, Pinschewer DD, Klenerman P, Rousson V, Gaboli M et al.** Effects of promyelocytic leukemia protein on virus-host balance. *J Virol* 2002;76(8):3810-3818.doi: 10.1128/jvi.76.8.3810-3818.2002
66. **Tavalai N, Papior P, Rechter S, Leis M, Stamminger T**. Evidence for a role of the cellular ND10 protein PML in mediating intrinsic immunity against human cytomegalovirus infections. *J Virol* 2006;80(16):8006-8018.doi: 10.1128/JVI.00743-06
67. **Blondel D, Regad T, Poisson N, Pavie B, Harper F et al.** Rabies virus P and small P products interact directly with PML and reorganize PML nuclear bodies. *Oncogene* 2002;21(52):7957-7970.doi: 10.1038/sj.onc.1205931
68. **El Bougrini J, Dianoux L, Chelbi-Alix MK**. PML positively regulates interferon gamma signaling. *Biochimie* 2011;93(3):389-398.doi: 10.1016/j.biochi.2010.11.005
69. **Scherer M, Klingl S, Sevvana M, Otto V, Schilling EM et al.** Crystal structure of cytomegalovirus IE1 protein reveals targeting of TRIM family member PML via coiled-coil interactions. *PLoS Pathog* 2014;10(11):e1004512.doi: 10.1371/journal.ppat.1004512
70. **Kim YE, Ahn JH**. Positive role of promyelocytic leukemia protein in type I interferon response and its regulation by human cytomegalovirus. *PLoS Pathog* 2015;11(3):e1004785.doi: 10.1371/journal.ppat.1004785
71. **Scherer M, Otto V, Stump JD, Klingl S, Muller R et al.** Characterization of Recombinant Human Cytomegaloviruses Encoding IE1 Mutants L174P and 1-382 Reveals that Viral Targeting of PML Bodies Perturbs both Intrinsic and Innate Immune Responses. *J Virol* 2016;90(3):1190-1205.doi: 10.1128/jvi.01973-15
72. **Spector DL, Lamond AI**. Nuclear speckles. *Cold Spring Harb Perspect Biol* 2011;3(2).doi: 10.1101/cshperspect.a000646
73. **McFarlane M, MacDonald AI, Stevenson A, Graham SV**. Human Papillomavirus 16 Oncoprotein Expression Is Controlled by the Cellular Splicing Factor SRSF2 (SC35). *J Virol* 2015;89(10):5276-5287.doi: 10.1128/jvi.03434-14
74. **Walker EJ, Younessi P, Fulcher AJ, McCuaig R, Thomas BJ et al.** Rhinovirus 3C protease facilitates specific nucleoporin cleavage and mislocalisation of nuclear proteins in infected host cells. *PLoS One* 2013;8(8):e71316.doi: 10.1371/journal.pone.0071316
75. **Parker JS, Broering TJ, Kim J, Higgins DE, Nibert ML**. Reovirus core protein mu2 determines the filamentous morphology of viral inclusion bodies by interacting with and stabilizing microtubules. *J Virol* 2002;76(9):4483-4496.doi: 10.1128/jvi.76.9.4483-4496.2002

76. **Zurney J, Kobayashi T, Holm GH, Dermody TS, Sherry B**. Reovirus mu2 protein inhibits interferon signaling through a novel mechanism involving nuclear accumulation of interferon regulatory factor 9. *J Virol* 2009;83(5):2178-2187.doi: 10.1128/jvi.01787-08
77. **Kar AK, Bhattacharya B, Roy P**. Bluetongue virus RNA binding protein NS2 is a modulator of viral replication and assembly. *BMC Mol Biol* 2007;8:4.doi: 10.1186/1471-2199-8-4
78. **Hu L, Crawford SE, Hyser JM, Estes MK, Prasad BV**. Rotavirus non-structural proteins: structure and function. *Curr Opin Virol* 2012;2(4):380-388.doi: 10.1016/j.coviro.2012.06.003
79. **Fernandez de Castro I, Zamora PF, Ooms L, Fernandez JJ, Lai CM et al.** Reovirus forms neo-organelles for progeny particle assembly within reorganized cell membranes. *mBio* 2014;5(1).doi: 10.1128/mBio.00931-13
80. **Desmet EA, Anguish LJ, Parker JS**. Virus-mediated compartmentalization of the host translational machinery. *mBio* 2014;5(5):e01463-01414.doi: 10.1128/mBio.01463-14
81. **Choudhury P, Bussiere LD, Miller CL**. Mammalian Orthoreovirus Factories Modulate Stress Granule Protein Localization by Interaction with G3BP1. *J Virol* 2017;91(21).doi: 10.1128/jvi.01298-17
82. **Dhillon P, Tandra VN, Chorghade SG, Namsa ND, Sahoo L et al.** Cytoplasmic Relocalization and Colocalization with Viroplasms of Host Cell Proteins, and Their Role in Rotavirus Infection. *J Virol* 2018;92(15).doi: 10.1128/jvi.00612-18
83. **Dhillon P, Rao CD**. Rotavirus Induces Formation of Remodeled Stress Granules and P Bodies and Their Sequestration in Viroplasms To Promote Progeny Virus Production. *J Virol* 2018;92(24).doi: 10.1128/jvi.01363-18
84. **Oksayan S, Wiltzer L, Rowe CL, Blondel D, Jans DA et al.** A novel nuclear trafficking module regulates the nucleocytoplasmic localization of the rabies virus interferon antagonist, P protein. *J Biol Chem* 2012;287(33):28112-28121.doi: 10.1074/jbc.M112.374694
85. **Audsley MD, Jans DA, Moseley GW**. Roles of nuclear trafficking in infection by cytoplasmic negative-strand RNA viruses: paramyxoviruses and beyond. *J Gen Virol* 2016;97(10):2463-2481.doi: 10.1099/jgv.0.000575
86. **Chen Z, Liu S, Sun W, Chen L, Yoo D et al.** Nuclear export signal of PRRSV NSP1alpha is necessary for type I IFN inhibition. *Virology* 2016;499:278-287.doi: 10.1016/j.virol.2016.07.008
87. **Janowicz A, Caporale M, Shaw A, Gulletta S, Di Gialleonardo L et al.** Multiple genome segments determine virulence of bluetongue virus serotype 8. *J Virol* 2015;89(10):5238-5249.doi: 10.1128/jvi.00395-15
88. **Huismans H, van Staden V, Fick WC, van Niekerk M, Meiring TL**. A comparison of different orbivirus proteins that could affect virulence and pathogenesis. *Vet Ital* 2004;40(4):417-425

9. Figures and tables

Table 1. AHSV reference* and field strains used in this study, and the type of NS4 protein encoded by each.

AHSV serotype	Strain	Isolate name	GenBank accession no.	NS4 type
AHSV-1	Reference		KF859992, AM883170	NS4-II
AHSV-2	Reference		KF860003	NS4-II
AHSV-3	Reference		KM886360	NLS-NS4-II
AHSV-4	Reference		KM609473	NS4-I
AHSV-5	Reference		KM886352	NS4-II
AHSV-6	Reference		KF860014	NS4-I
AHSV-7	Reference		KF860024	NS4-II
AHSV-8	Reference		KF860034	NS4-II
AHSV-9	Reference		KF860044	NS4-II
AHSV-1	Field	DM21/11	MN625126	NS4-II
AHSV-2	Field	DM8/14	MN625127	NS4-II
AHSV-3	Field	DM10/13	MN625128	NS4-I
AHSV-4	Field	DM10/14	MN625129	NS4-I
AHSV-5	Field	62/07/05 (Bailey)	MN625130	NS4-I
AHSV-6	Field	DM9/14	MN625131	NS4-II
AHSV-7	Field	DM9/15	MN625132	NS4-I
AHSV-8	Field	DM5/15	MN625133	NLS-NS4-II
AHSV-9	Field	DM12/14	MN625134	NS4-II

* The isolation history and Seg-9 sequences of the AHSV reference strains have been described previously [21, 30]

Table 2. Recombinant baculoviruses used in this study

Baculovirus	**Protein expressed**	**AHSV strain**	**Genbank nr of Seg-9 sequence**	**Primer sequences (5' – 3')**
Bac-NS4-I	NS4-I	AHSV-4 Ref	KM609473	NS4-I FP: ATAGGATCCGATGGAGGATTGGGATCAGC NS4-I RP: CCAAGCTTCTAATCCCCCATCCCGTC
Bac-NS4-II	NS4-II	AHSV-3 Field	KP009647	NS4-II FP: AAGGATCCTATGATGATCGAAGAGTGGA NS4-II RP: GGAAGCTTCTAATCCTCCAATCCGTCTA
Bac-NLS-NS4-II	NLS-NS4-II	AHSV-3 Ref	KM886360	NLS-NS4-II FP: AGGGATCCGATGGGGAGAAGAAGAAC NLS-NS4-II RP: ATCAAGCTTCTAATCCTCCAATCC
Bac-Seg-9	NLS-NS4-II and VP6	AHSV-3 Ref	KM886360	
Bac-eGFP	eGFP			
Bac-NLS-NS4-I	NLS-NS4-I	AHSV-4 Ref		NS4-I FP: AAGAGAACAAAATAC ATGGAGGATTGGGATCAGCAAAATC NS4-I RP: CTTCTCGACAAGCTT CTAATCCCCCATCCCGTCGA
Bac-NLS-eGFP	NLS-eGFP			eGFP FP: AAGAGAACAAAATAC GTGAGCAAGGGCGAGGAGCTGTTCA eGFP RP: CTTCTCGACAAGCTT TTACTTGTACAGCTCGTCCATGCCG pFB-NLS FP:AAGCTTGTCGAGAAG TACTA pFB-NLS RP: GTATTTTGTTCTCTT CCTTTTCACTC

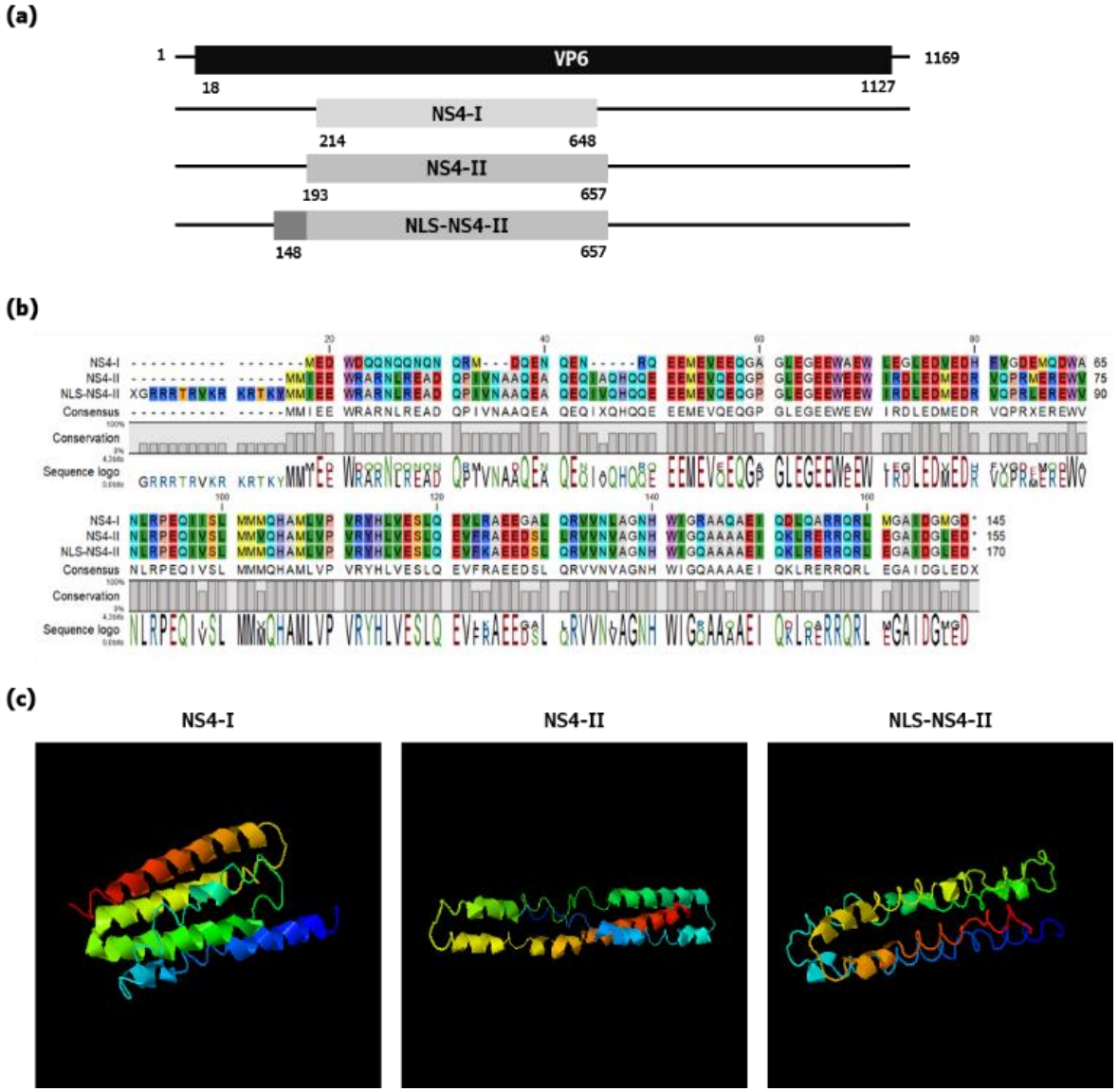

Fig. 1. (a) Schematic representation of the relative positions of the open reading frames of VP6 and all NS4 types (NS4-I, NS4-II and NLS-NS4-II) on Seg-9 (solid black line). **(b)** Amino acid sequence alignment and conservation plots of the NS4 proteins encoded by AHSV-4 Field (NS4-I), AHSV-1 Field (NS4-II) and AHSV-8 Field (NLS-NS4-II) strains. **(c)** The predicted 3D model of NS4-I (C-score = -2.54; TM-score = 0.42 ± 0.14), NS4-II (C-Score = -1.45; TM-score = 0.54 ± 0.15 and NLS-NS4-II (C-score = -2.72; TM-score = 0.40 ± 0.14). N-terminal and C-terminal shown in blue and red respectively.

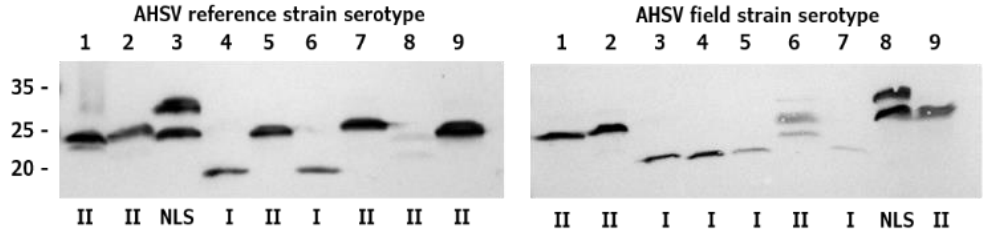

Fig. 2. Immunoblot demonstrates NS4 expression from all AHSV strains. Cell lysates of BSR-T7 cells infected with each of the nine AHSV reference or field strains respectively were subjected to SDS-PAGE/Western blot using anti-NS4 (Genscript) serum. The numbers at the top of each image represents the AHSV serotype, and the roman numerals at the bottom indicates the NS4 type; I = NS4-I, II = NS4-II, NLS = NLS-NS4-II. Size markers are indicated on the left in kDa.

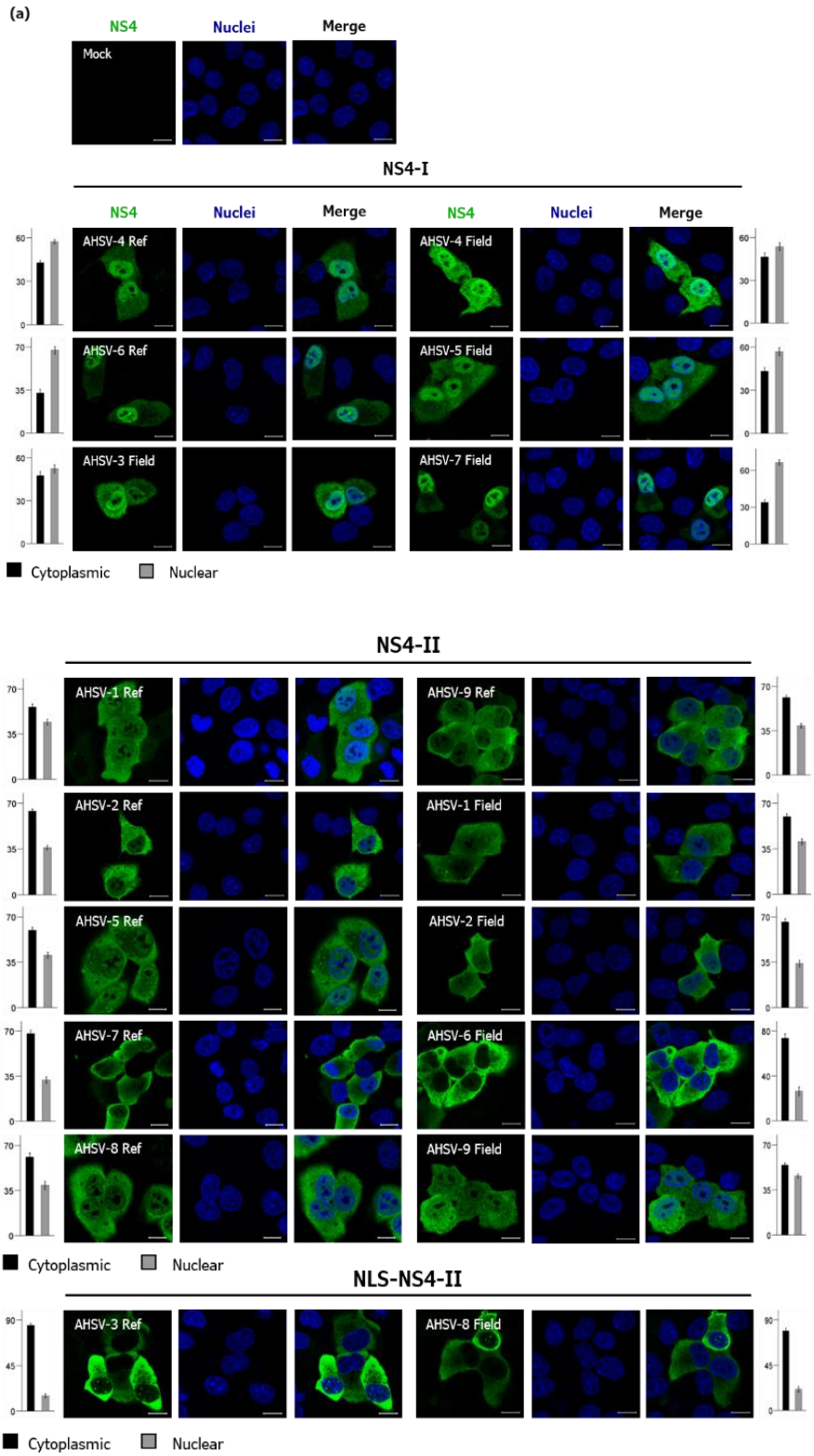
(a)
NS4
Nuclei
Merge
Mock
NS4-I
NS4
Nuclei
Merge
NS4
Nuclei
Merge
AHSV-4 Ref
AHSV-4 Field
AHSV-6 Ref
AHSV-5 Field
AHSV-3 Field
AHSV-7 Field
Cytoplasmic
Nuclear
NS4-II
AHSV-1 Ref
AHSV-9 Ref
AHSV-2 Ref
AHSV-1 Field
AHSV-5 Ref
AHSV-2 Field
AHSV-7 Ref
AHSV-6 Field
AHSV-8 Ref
AHSV-9 Field
Cytoplasmic
Nuclear
NLS-NS4-II
AHSV-3 Ref
AHSV-8 Field
Cytoplasmic
Nuclear

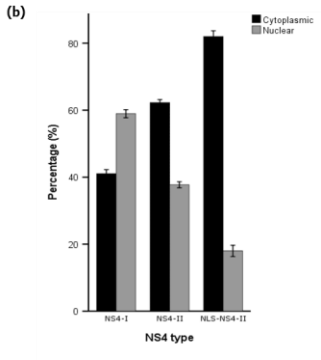

Fig. 3. Indirect immunofluorescence microscopy reveals that the intracellular localisation of NS4 displays three different patterns. (a) AHSV-infected BSR-T7 cells were fixed at 24 hpi and labelled with anti-NS4 (E3F) primary and Alexa Fluor 488 secondary antibody (green) and viewed by CLSM. Nuclei were counterstained with DAPI (blue). Images are grouped according to the NS4 type encoded by the respective AHSV strain. Scale bars represent 10 µm. Bar graphs showing the mean cytoplasmic and nuclear percentages of NS4 of each strain are indicated on either side of each image. **(b)** Graph depicting the mean cytoplasmic and nuclear percentages of each NS4 type. All graphs represent samples from at least two independent experiments and a minimum of 40 cells analysed per strain. Standard deviations for each strain are shown as error bars.

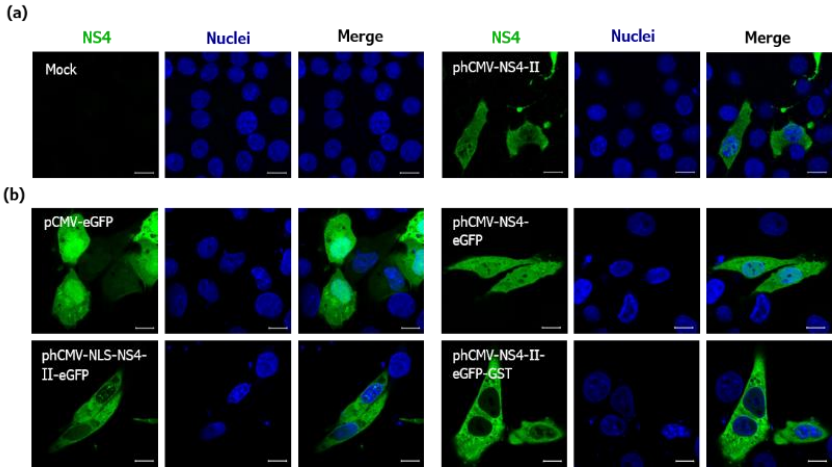

Fig. 4. Indirect immunofluorescence microscopy of transfected cells indicates nuclear entry of NS4 via passive diffusion. BSR cells were **(a)** mock-transfected or transfected with phCMV-NS4-II and labelled with anti-NS4 (Genscript) or **(b)** transfected with pCMV-eGFP, phCMV-NS4-eGFP, phCMV-NLS-NS4-II-eGFP or phCMV-NS4-II-eGFP-GST and fixed 48 hours post transfection and viewed by CLSM. Nuclei were counterstained with DAPI (blue). Scale bars represent 10 µm.

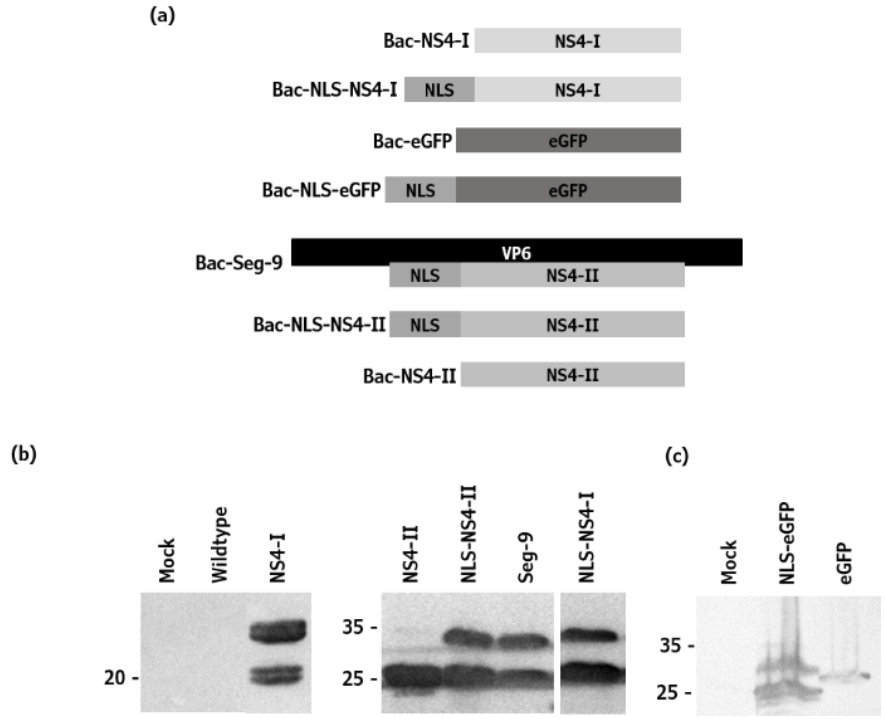

Fig. 5. Confirmation of expression of different NS4 proteins from recombinant baculoviruses. (a) Schematic representation of proteins expressed from all recombinant baculoviruses used. **(b)** Recombinant baculoviruses expressing different NS4 types as indicated were used to infect Sf9 cells, lysates of cells harvested at 48 hpi were analysed by 15% SDS-PAGE and Western blot with **(b)** anti-NS4 (Genscript) serum or **(c)** anti-eGFP serum. Protein sizes are indicated on the left in kDa. Negative controls include mock-infected or wildtype baculovirus-infected cells.

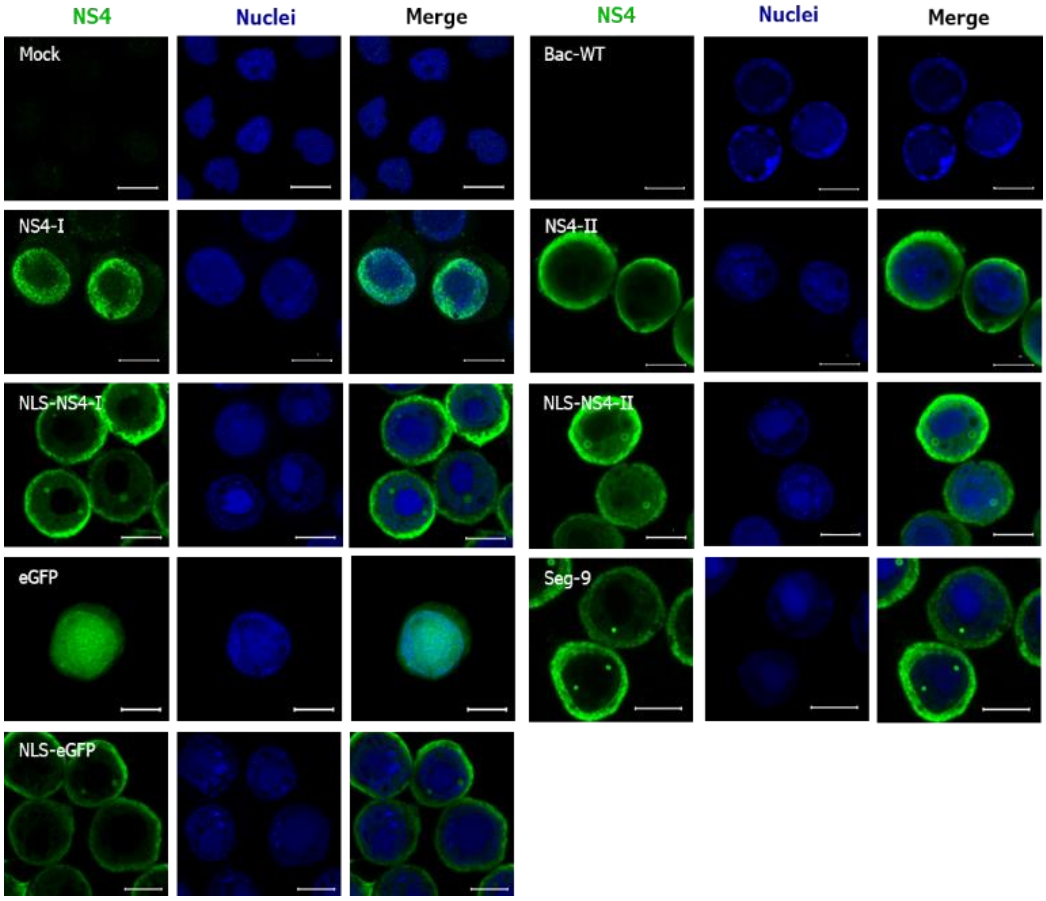

Fig. 6. The intracellular distribution of AHSV NS4 remains the same in the absence of other AHSV proteins. Sf9 cells were mock-infected or infected with wild type baculovirus (Bac-WT) or recombinant baculoviruses Bac-NS4-I, Bac-NS4-II, Bac-Seg-9, Bac-VP6-NLS-NS4-II, Bac-NLS-NS4-I, Bac-NLS-NS4-II, Bac-eGFP or Bac-NLS-eGFP expressing the corresponding type of NS4. Cells were fixed at 30 hpi and immunolabelled with anti-NS4 (Genscript) and AlexaFluor 488 secondary antibody (green) and viewed by CLSM. Nuclei were counterstained with DAPI (blue). Scale bars represent 10 µm.

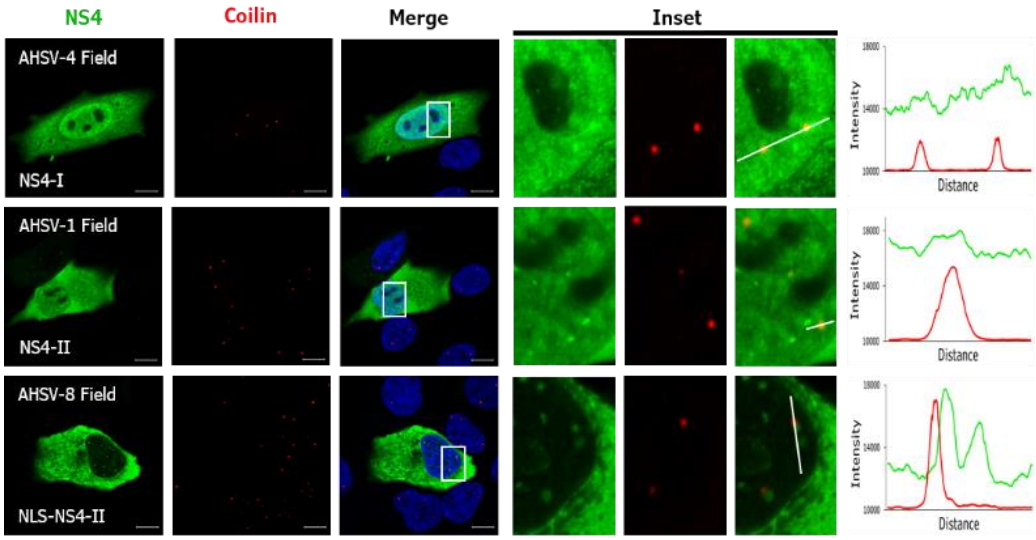

Fig. 7. AHSV NS4 does not colocalise with Cajal bodies. HeLa cells were infected with AHSV strains as indicated, fixed and dual immunolabelled at 24 hpi with anti-NS4 (E3F) and anti-coilin primary and AlexaFluor-488 (green) and AlexaFluor-594 (red) secondary antibodies, respectively. Nuclei were counterstained with DAPI (blue). The area demarcated by the white block in the merged image is enlarged in the inset panel. Histograms display the fluorescence intensity values of NS4 (green) and coilin (red) measured along the white line drawn in the inset panels. Scale bars represent 10 µm.

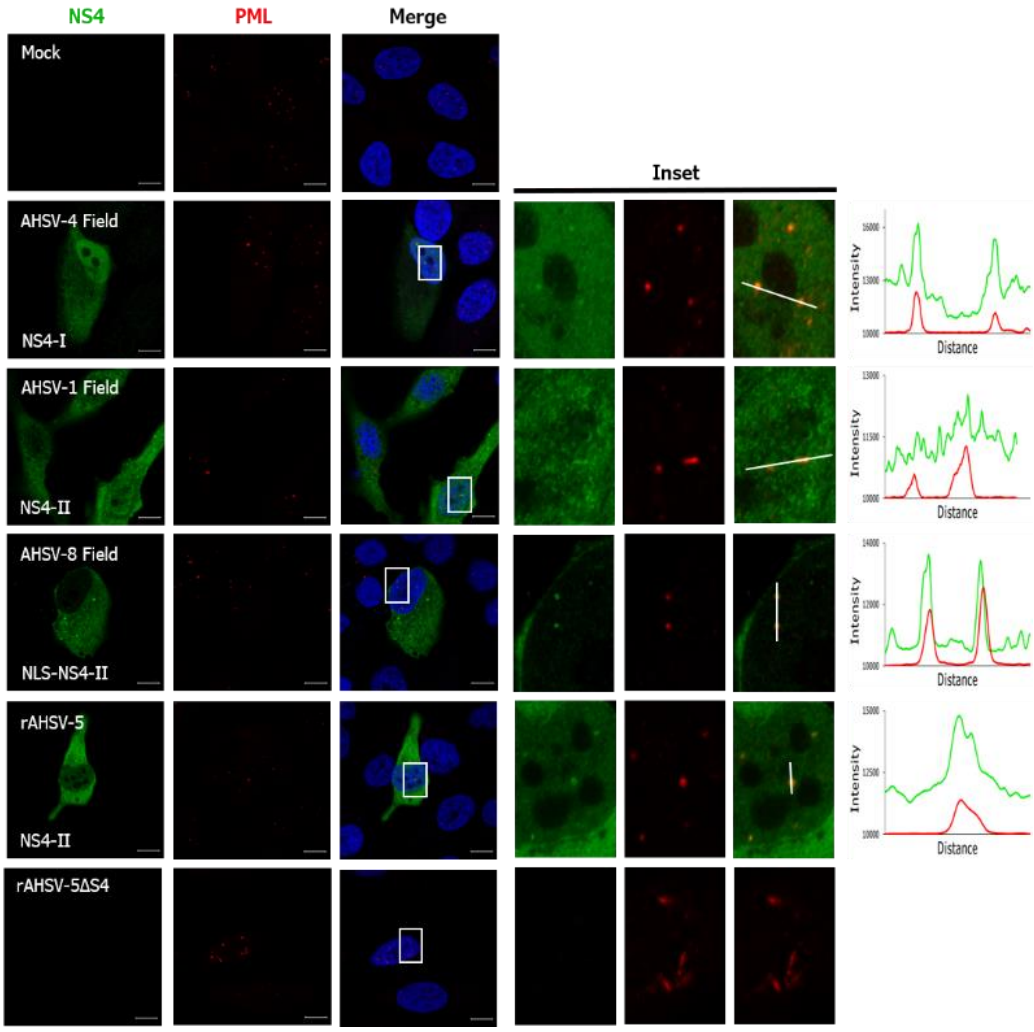

Fig. 8. AHSV NS4 colocalises with PML-NBs. HeLa cells were infected with different AHSV strains as indicated, fixed and dual immunolabelled at 24 hpi with anti-NS4 (E3F) and anti-PML primary and AlexaFluor 488 (green) and AlexaFluor 594 (red) secondary antibodies respectively. Nuclei were counterstained with DAPI (blue). The area demarcated by the white block in the merged image is enlarged in the inset panel. Histograms display the fluorescence intensity values of NS4 (green) and PML (red) measured along the white line drawn in the inset panels. Scale bars represent 10 µm.

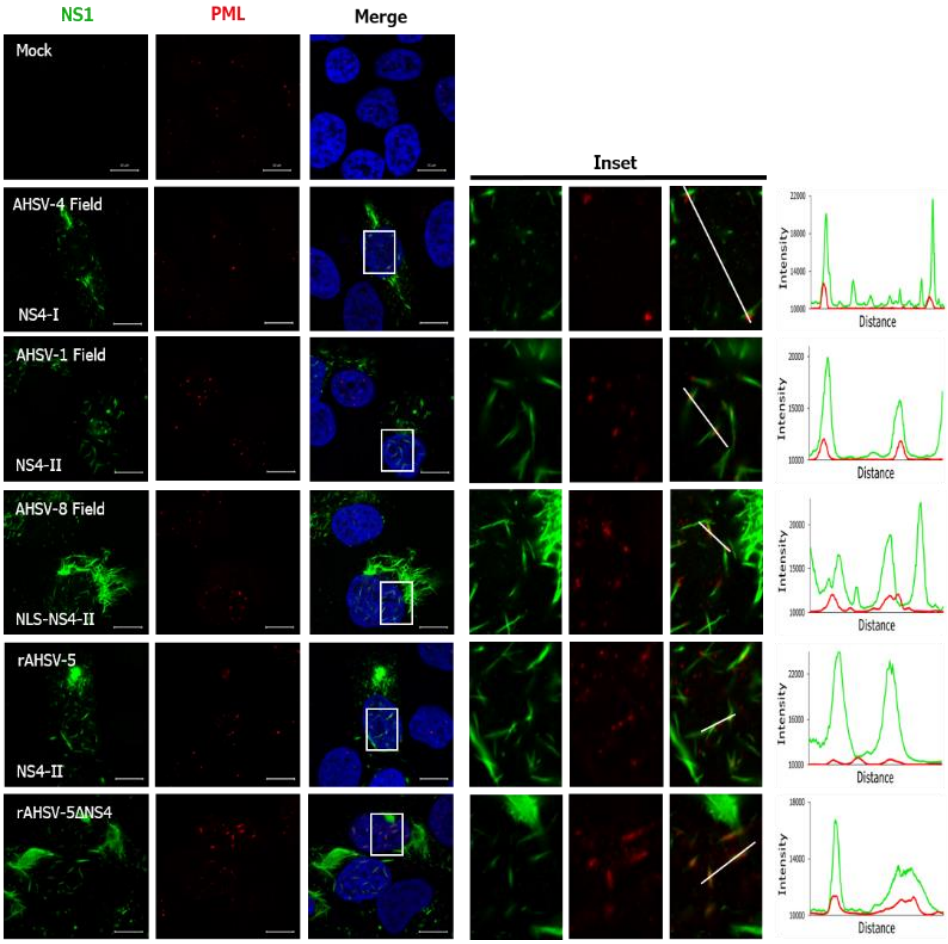

Fig. 9. NS1 associates closely with PML-NBS. BSR-T7 cells were mock- or AHSV-infected as indicated, fixed and immunolabelled at 24 hpi with anti-NS1 and anti-PML primary and AlexaFluor 488 (green) and AlexaFluor 594 (red), secondary antibodies, respectively. Nuclei were counterstained with DAPI (blue). The area demarcated by the white block in the merged image is enlarged in the inset panel. Histograms display the fluorescence intensity values of NS1 (green) and PML (red) measured along the white line drawn in the inset panels. Scale bars represent 10 µm.

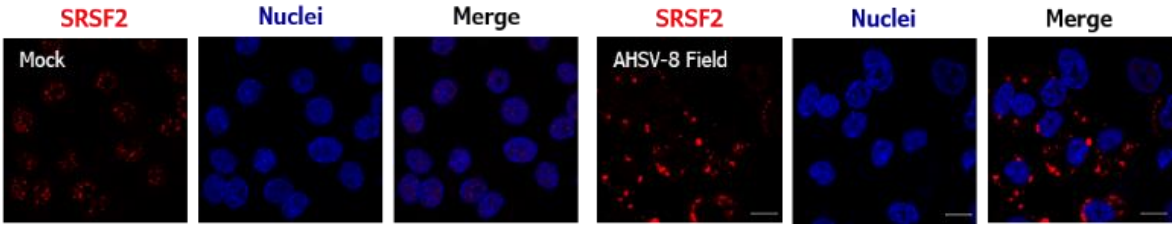

Fig. 10. SRSF2 relocates to the cytoplasm during AHSV infection. BSR-T7 cells were mock- or AHSV-infected as indicated, fixed and immunolabelled at 24 hpi with anti-SRSF2 primary and AlexaFluor 594 (red) secondary antibodies. Nuclei were counterstained with DAPI (blue). Scale bars represent 10 µm.

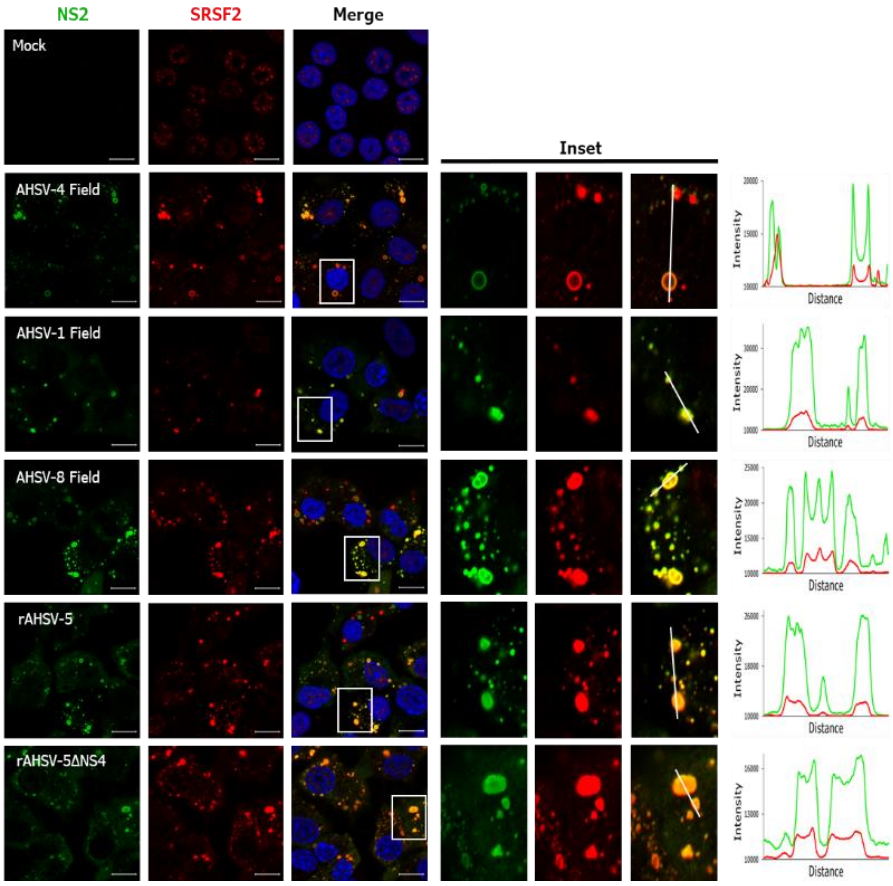

Fig. 11. SRSF2 colocalises with AHSV NS2 in VIBs. BSR-T7 cells were infected with different AHSV strains as indicated, fixed and dual immunolabelled at 24 hpi with anti-NS2 and anti-SRSF2 primary and AlexaFluor 488 (green) and AlexaFluor 594 (red) secondary antibodies respectively. Nuclei were counterstained with DAPI (blue). The area demarcated by the white block in the merged image is enlarged in the inset panel. Histograms display the fluorescence intensity values of NS2 (green) and SRSF2 (red) measured along the white line drawn in the inset panels. Scale bars represent 10 µm.

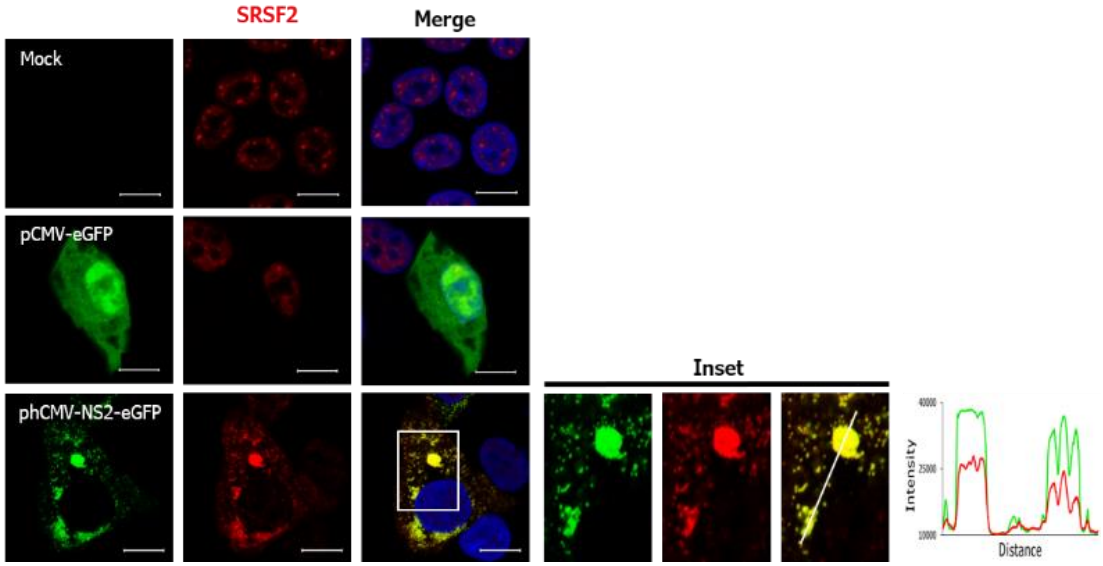

Fig. 12. SRSF2 colocalises with AHSV NS2 in VIB-like foci formed during transient NS2 expression. BSR-T7 cells were mock- or plasmid-transfected as indicated, fixed and immunolabelled at 48 hpt. Cells were labelled was with anti-SRSF2 primary and AlexaFluor 594 (red) secondary antibodies. Nuclei were counterstained with DAPI (blue). The area demarcated by the white block in the merged image is enlarged in the inset panel. The histogram displays the fluorescence intensity values of NS2-eGFP (green) and SRSF2 (red) measured along the white line drawn in the inset panel. Scale bars represent 10 µm.